Canards and curvature: nonsmooth approximation by pinching

M Desroches and M R Jeffrey

University of Bristol, Department of Engineering Mathematics, Queen's Building, University Walk, Bristol BS8 1TR, UK

E-mail: M.Desroches@bristol.ac.uk, Mike.Jeffrey@bristol.ac.uk

Abstract. In multiple time-scale (singularly perturbed) dynamical systems, *canards* are counterintuitive solutions that evolve along both attracting and repelling invariant manifolds. In two dimensions, canards result in periodic oscillations whose amplitude and period grow in a highly nonlinear way: they are slowly varying with respect to a control parameter, except for an exponentially small range of values where they grow extremely rapidly. This sudden growth, called a *canard explosion*, has been encountered in many applications ranging from chemistry to neuronal dynamics, aerospace engineering and ecology. Canards were initially studied using nonstandard analysis, and later the same results were proved by standard techniques such as matched asymptotics, invariant manifold theory and parameter blow-up. More recently, canard-like behaviour has been linked to surfaces of discontinuity in piecewise-smooth dynamical systems.

This paper provides a new perspective on the canard phenomenon by showing that the nonstandard analysis of canard explosions can be recast into the framework of piecewise-smooth dynamical systems. An exponential coordinate scaling is applied to a singularly perturbed system of ordinary differential equations. The scaling acts as a lens that resolves dynamics across all time-scales. The changes of local curvature that are responsible for canard explosions are then analyzed. Regions where different time-scales dominate are separated by hypersurfaces, and these are *pinched* together to obtain a piecewise-smooth system, in which curvature changes manifest as discontinuity-induced bifurcations. The method is used to classify canards in arbitrary dimensions, and to derive the parameter values over which canards form either small cycles (canards without head) or large cycles (canards with head).

1. Introduction

This paper revisits the geometry of dynamical systems exhibiting relaxation oscillations. Extreme changes of flow curvature brought about by the presence of different time-scales are studied. After discussing previous approaches, we introduce new methods to characterize these changes. We show that a correspondence exists between certain singularities of current interest in two different kinds of dynamical system: those that are singularly perturbed [18], and those that are piecewise-smooth [9].

A system with two time-scales can typically contain regions of fast dynamics, evolving rapidly towards lower dimensional manifolds where regimes of slow dynamics take over. The stability of a slow manifold depends on it being hyberbolically attractive in its normal direction [7, 8, 18, 19]. The occurrence of *non*-hyperbolic points leads to the separation of the fast and slow dynamics becoming indistinct. This is well-known to generate such nontrivial behaviours as relaxation oscillations and canard explosions [28]. The term "canard" alludes to the duck-like shape of cycles that wrap around critical manifolds of a typically cubic form (look ahead to figure 2 panel ②), but also to the deception they play on the mathematician by their sudden appearance and disappearance. The explosion is a cascade of cycle growth that occurs in a parameter range that is exponentially small in the ratio between time-scales (a small parameter ε), implying that it is very difficult to observe either in practical or numerical situations, hence it could easily be construed as a discontinuous event. How small the time-scale ratio (ε) must be for this to occur is addressed in a related paper [6]. In this paper we show how such a discontinuous description can be derived, and still preserve sufficient geometry to capture the canard phenomenon in detail.

An extreme view of a slow-fast dynamical system can be taken by expressing it in terms of ordinary differential equations containing discontinuities. A vector field defines evolution throughout phase space, but its value can jump discontinuously across a surface called a switching manifold. In the systems we will consider, orbits can slide along the switching manifold in a manner that approximates the slow dynamics, while fast dynamics takes place outside the switching manifold. The conventional description of dynamics in piecewise-smooth vector fields was laid down by Filippov [9]. We will rederive Filippov's convention by different means, defining it as a piecewise-smooth union of vector fields of the fast and slow subsystems, combined with a map that 'pinches' phase space in the neighbourhood of the critical manifold. The pinching creates a hypersurface, the switching manifold, and the slow dynamics slides around inside it.

The pinched system compresses the cascade of cycles in a canard explosion into a single instant. We make a precise connection between this pinching formalism and the methods of nonstandard analysis applied to singular perturbation theory [1]. We begin by combining pinching with the nonstandard concept of an exponential microscope, and we show that approximations obtained by both methods are equivalent. Furthermore, an observation from [1] allows us to make successive approximations that separate the canard explosion into two cascades – one with small cycles ("canard without head") and one with large cycles ("canard with head") – each of which is instantaneous in the pinched system.

We demonstrate the pinching method on a classic example of a slow-fast system, namely the two-dimensional van der Pol oscillator [26]. We then apply pinching to a

system with two fast variables and one slow, which allows for oscillations on the fast time-scale observed as "bursting" oscillations. This is the classical Hindmarsh-Rose burster [13], where a spike-adding mechanism takes place and is organised by saddle-type canard cycles. The same mechanism can be found in other three-dimensional bursters (such as the Morris-Lecar equations [25]) and has been recently studied from the standpoint of invariant manifolds, in particular, slow manifolds of saddle-type and their (un)stable manifolds [11]. We demonstrate that, by using pinching microscope, one can understand the transition from canard cycles to spiking periodic attractors, that is, limit cycles with one spike.

The systems we analyse can all be expressed in the form

$$\varepsilon\ddot{x} + \dot{x}f'(x) = g(x, y, z), \tag{1}$$

where ε is a small positive constant, and f' is the x-derivative of a smooth function f, which is a cubic polynomial in x. The function g depends on x, and on a variable

$$y = \varepsilon\dot{x} + f(x), \tag{2}$$

and may depend on a third dynamic variable z. We can then write (1) as a system of ordinary differential equations,

$$\varepsilon\dot{x} = y - f(x), \tag{3a}$$

$$\dot{y} \ = g(x, y, z), \tag{3b}$$

from which it is clear that, for $\varepsilon \ll 1$, the dynamics will separate into a slow time-scale t and a fast time-scale t/ε. In cases where we have a third equation $\dot{z} = k(x, y, z)$, the dynamics of z may have either a fast or slow time-scale; the example we consider in section 4.3 falls into the first category.

The paper is arranged as follows. In section 2 we introduce some classic canard theory based on singularly perturbed systems, including the nonstandard analysis concept of an exponential microscope. Then in section 3 a description of canards in terms of pinched (or piecewise-smooth) vector fields is introduced, and applied to examples in section 4. In sections 4.1 and 4.2 we consider supercritical and subcritical cases of the van der Pol oscillator, the latter representing an abstract form of the Fitzugh-Nagumo equations, and in section 4.3 we apply the method to describe the birth of spiking via canard cycles in a three dimensional Hindmarsh-Rose model. In section 5 we apply pinching to derive a piecewise-smooth description of non-hyperbolic singularities and some of their related canards. Some concluding remarks are made in section 6.

2. The classic canard example

2.1. The van der Pol equations in the Liénard plane

Results in this section derive from the seminal paper on canards published by the French group from Strasbourg in the early 1980's [1]. Thoughout, they consider the equations of the van der Pol oscillator, which can be written as

$$\varepsilon\dot{x} = y - \frac{1}{3}x^3 + x, \tag{4a}$$

$$\dot{y} \ = q - x, \tag{4b}$$

in the Liénard plane (x, y) [21], with constant forcing q and singular perturbation parameter $0 < \varepsilon \ll 1$.

The system (4) exhibits a supercritical Hopf bifurcation as q passes through $q = \pm 1$, that is, a stable focus-type equilibrium loses stability by creation of a stable periodic orbit. The location of the small parameter ε in (4) distinguishes the nullcline $\dot{x} = 0$, which we label S_0 and call the critical manifold. It consists of attracting and repelling branches, S^a and S^r, adjoined at the turning points (or folds) of S_0, at $(x, y) = \pm(1, -\frac{2}{3})$, such that $S_0 = S^a \cup S^r$.

Let us first consider how the critical manifold organises the dynamics of the system for $\varepsilon = 0$, illustrated in figure 1. Setting $\varepsilon = 0$ in (4) gives a differential-algebraic system consisting of the differential equation $\dot{y} = q - x$ on the slow time-scale, constrained to S_0 by the algebraic equation $y = x^3/3 - x$. Hence S_0 is the phase space of this limiting problem, called the "slow subsystem" (or sometimes "reduced system").

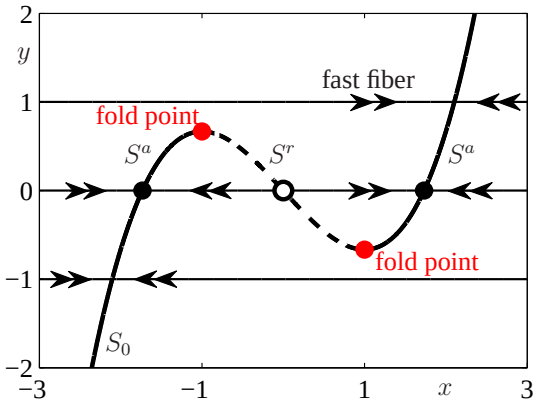

Figure 1. Fast and slow subsystems of the van der Pol equation. Double arrows indicate a fast motion. The fold points of the critical manifold S_0 correspond to the bifurcation points of the fast dynamics; they separate the attracting sheets S^a of the critical manifold from the repelling sheet S^r.

To study the fast subsystem one introduces a fast time-scale $\tau = t/\varepsilon$. Denoting differentiation with respect to τ by a prime, (4) becomes

$$x' = y - \frac{1}{3}x^3 + x, \tag{5a}$$

$$y' = \varepsilon(q - x). \tag{5b}$$

When $\varepsilon = 0$, the slow variable y has its dynamics frozen, that is, y remains constant and can be considered as a parameter. This yields a family of one-variable differential equations on the fast time-scale, parametrised by y and usually referred to as the "fast subsystem" (or sometimes "layer problem"). The full system with $\varepsilon = 0$ is piecewise-smooth, with a switch occurring between the fast and slow subsystems. From (5a) we observe that the (y-parameterized) equilibria of the fast subsystem belong to none other than the critical manifold S_0, being stable on S^a and unstable on S^r (indicated by the filled and unfilled disks in figure 1).

The aim in this paper, as in singular perturbation theory, is to build from this insight on the limiting case $\varepsilon = 0$ to study what happens when ε is small but nonzero. Here we recount the main results, summarized in figure 2, which shows a simulation of (4) for $\varepsilon = 5 \times 10^{-3}$. If an initial condition is taken a distance of $\mathsf{O}(1)$ away

from the critical manifold S_0, the solution of the van der Pol equation first evolves on a fast time-scale, almost horizontally, until it reaches an ε-neighbourhood of one of the attracting sheets S^a. This first epoch is well captured by the fast subsystem of horizontal fibres in figure 1. Once in the neighbourhood of S^a, where $\dot{x} \approx 0$, the slow subsystem begins to dominate the dynamics and the orbit moves slowly, close to S^a. The sole event that can end this slow epoch is a loss of normal stability of the attracting sheet S^a of the critical manifold. This corresponds to a bifurcation point of the fast subsystem, generically a saddle-node bifurcation, and takes place at either of the folds in figure 1.

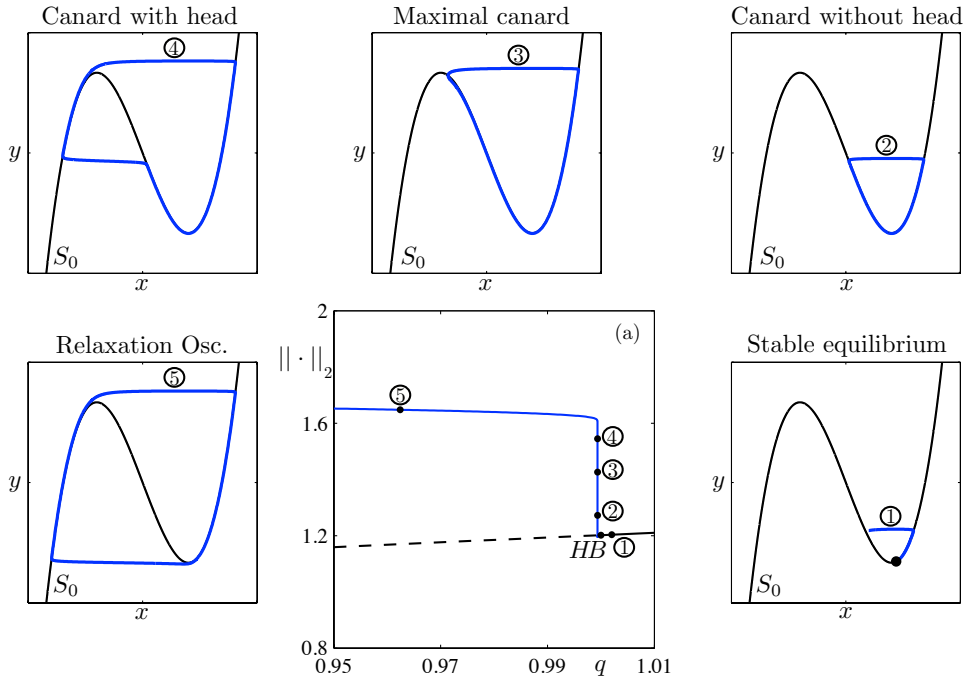

Figure 2. Canard explosion in the van der Pol system. The central panel (a) shows the bifurcation diagram of this system as a function of the parameter q (L_2-norm $||\cdot||$ of the limit cycle on the upper branch, and equilibria along the lower branch, unstable on the dashed part to the left of *HB*). The quasi-vertical part of the branch of limit cycles corresponds to the canard explosion. Five dots (other than the Hopf point *HB*) are marked along the branch: ① is a stable equilibrium solution and ② to ⑤ are periodic solutions, of which ② to ④ are canards and ⑤ is a relaxation oscillation. The five solutions are represented in the state space (x, y) in the outer panels, together with the cubic nullcline S_0.

A simple stability analysis of (4) reveals a unique fixed point where $\dot{x} = \dot{y} = 0$, which lies on S_0 for all q. For $|q| > 1$ the fixed point is stable and lies on S^a, for $|q| < 1$ it is unstable and lies on S^r. When $q = \pm 1$, the system undergoes a Hopf bifurcation which takes place at the fold of S_0, creating a branch of stable periodic orbits that displays the so-called "canard explosion". A surprising property of the canards becomes clear when one plots orbits for various values of q together with the critical manifold S_0 in the Liénard plane. As shown in figure 2, a periodic orbit follows the attracting sheet S^a of the critical manifold down to the fold point, then, counterintuitively, instead of being ejected at the fold along a fast fibre, the orbit

sticks to S_0 along its repelling sheet S^r for an $\mathsf{O}(1)$ time.

The family of canard cycles are distinguished as being "with head" or "without head" as in figure 2. The distinction depends on whether an orbit leaves the ε-neighbourhood of S^r along a fast fibre moving to the left (with head) or to the right (without head) as depicted. The intervening case occurs at a parameter value $q = q_0$ and is called the *maximal canard*, shown in panel 3 of figure 2. The maximal canard follows the unstable region for the greatest time possible by traveling the whole length of S^r between the folds. The value of q_0 can be estimated numerically or calculated analytically using asympotic expansions in ε (e.g. [2]), and in section 4.1 we estimate it geometrically.

To understand why the canards stick to the repelling critical manifold S^r, it is usual to consider them from the viewpoint of invariant manifolds. In the singular limit $\varepsilon = 0$, S_0 is an invariant manifold. The question of the persistence of invariant manifolds for $\varepsilon > 0$ was addressed in the 1970's in the work of Hirsh, Pugh and Shub [14] and, in the context of slow-fast dynamical systems, in the work of Fenichel [7, 8]; see also [18, 19]. Fenichel proved that compact normally hyperbolic subsets of an invariant manifold, such as S_0 in the present case, persist as locally invariant manifolds S_ε (generally non-unique) for every small enough $\varepsilon > 0$, and that they are smooth ε-perturbations of the unperturbed manifold. Normal hyperbolicity can be lost, however, as happens generically at (isolated) fold points in planar systems, where attracting and repelling sheets of invariant manifolds intersect. Therefore, in the case of the one-dimensional cubic critical manifold S_0, one can apply Fenichel theory everywhere except the fold points.

The key to the canard explosion is the fact that a small parameter change can alter the arrangement of the attracting and repelling branches S^a_ε and S^r_ε of the invariant manifold S_ε. Specifically, the size of a canard cycle is determined by whether the arrangement of S^a_ε and S^r_ε forces it to curve inside the critical manifold S_0 (figure 3(a)) to form a canard without head, or outside it (figure 3(c)) to form a canard with head. Since the two invariant manifolds exchange their position between figures 3 (a) and

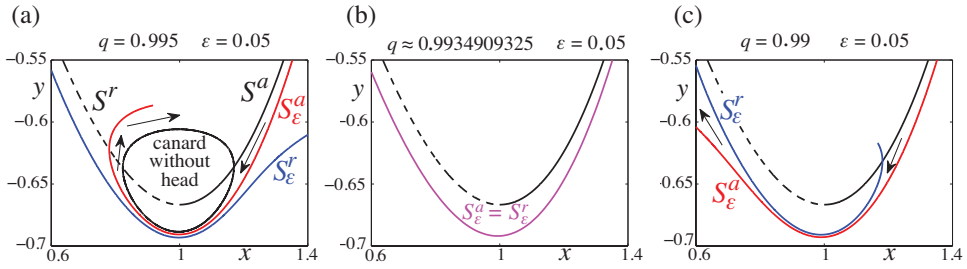

Figure 3. Invariant manifolds in the neighbourhood of the fold during the canard explosion. Showing the attracting and repelling invariant manifolds S^a_ε and S^r_ε, and the critical manifold $S_0 = S^a \cup S^r$, for different values of q. In (a), S^a_ε curves inside S^r_ε allowing for a small canard cycle; in (b), S^a_ε and S^r_ε coincide; in (c), the two manifolds have exchanged their positions and the resulting periodic attractor is a large canard cycle.

(b) as q varies, there must exist a parameter value $q = q_0$ at which they pass through each other. Then, as the manifolds are themselves orbits, they must coincide as shown in figure 3(b). The canard that passes from S^a_ε to S^r_ε will remain on the repelling sheet S^r for the longest distance possible, creating the maximal canard shown in panel ③

of figure 2. The strong (exponential) repulsion in the normal direction from S^r_ε causes the transition between small (without head) and large (with head) canard cycles to occur within an interval of q that is of order $e^{-c/\varepsilon}$ for some $c > 0$. This implies that it is not trivial to resolve different canard cycles, because their repelling segments are all contained in an exponentially small thickness around S^r. In order to obtain quantitative as well as qualitative information about the canards along the explosive bifurcation branch, changes of coordinate were introduced in [1] that magnify the geometry close to S^r, such that different canards within the same subfamily (i.e. with or without head) can be separated. The crucial point is that this magnification must be exponentially strong in ε in order to distinguish between orbits that are exponentially close to each other, as we show in the following section.

2.2. Exponential microscope

To understand relaxation oscillations in more detail we must separate the canard cycles, figure 2, from the critical manifold, S_0. We follow [1] by defining a new variable, $v = \dot{x}$, which has the effect of stretching the phase portrait by a factor of $1/\varepsilon$ in the direction transverse to S_0. In the (x, v) plane, (4) becomes

$$\dot{x} = v, \tag{6a}$$

$$\varepsilon\dot{v} = q - x - (x^2 - 1)v. \tag{6b}$$

The dynamics in these coordinates is somewhat changed in appearance, however it is clear that there is a one-to-one correspondence between orbits of the van der Pol system in the Liénard plane (x, y) and in the phase plane (x, v). In these coordinates x is a slow variable compared to v, so the slow dynamics is organised around a critical manifold $\dot{v} = 0$, (in place of S_0 which is now the $v = 0$ axis), given by

$$S_v = \{(x, v) \ : \ v = \gamma(x)\}, \quad \text{where} \quad \gamma(x) \equiv \frac{q - x}{x^2 - 1}. \tag{7}$$

The change to coordinates (x, v) implements a magnification transverse to S_0 by a factor ε. Although this separates the canard cycles from S_0 (as we shall see in section 4.1), it is not strong enough to separate canard cycles from each other, and in particular cannot resolve the maximal canard. To this end, Benoît et al. introduced an *exponential microscope*. For this stronger magnification we must do better than zooming in on S_0. As observed in [1], the maximal canard can be approximated near the fold by S_v when $q = 1$, which by (7) is given the hyberbola $v = \gamma_0(x) \equiv -\frac{1}{1+x}$. Thus the required 'microscope' variable is defined as

$$w = (v - \gamma_0(x))^{[\varepsilon]}, \tag{8}$$

employing the notation

$$x^{[p]} \equiv |x|^p \mathrm{sgn}(x) \tag{9}$$

which will recur throughout the paper. As was found in [1] (and we rederive in section 4.1) using $\dot{w} = \frac{dw}{dt} \cdot \frac{dt}{dx}$ and letting $\delta = (q - q_0)^{[\varepsilon]}$, we now have

$$\dot{x} = w^{[1/\varepsilon]} + \gamma_0, \tag{10a}$$

$$\dot{w} = w\left(\frac{x - q_0}{\gamma_0} + \left(\frac{\delta}{w}\right)^{[1/\varepsilon]}\right), \tag{10b}$$

recalling that q_0 is defined as the parameter value for which the canard is maximal (figure 2 panel ③).

The term $w\,(\delta/w)^{[1/\varepsilon]}$ is a perturbation of the $\delta = 0$ (maximal canard) system. It is small for $|w| \gg \delta$, where the perturbation is negligible, but in the strip $|w| \ll \delta$ this term dominates and the vector field is almost vertical. The illustration of this in figure 4 is based on the original analysis in [1], which can be summarized as follows.

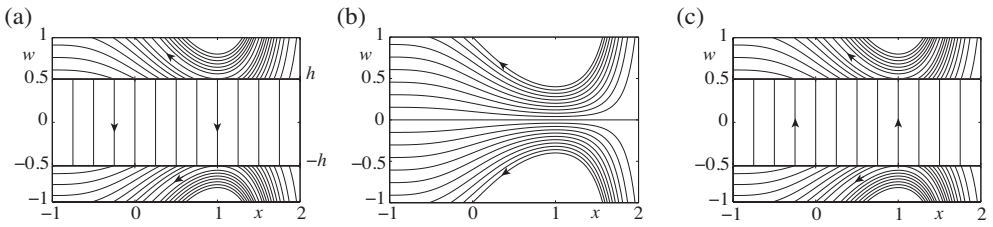

Figure 4. The van der Pol system under the exponential microscope: (a) $q < q_0$, ($\delta < 0$), (b) $q = q_0$, ($\delta = 0$), (c) $q > q_0$, ($\delta > 0$).

In the parameter regime of the canard explosion, asymptotic analysis reveals that $\delta = q - q_0 = \exp(-c/\varepsilon)$ for a constant $c > 0$, guaranteeing that $\delta \ll 1$. At the parameter value $q = q_0$, when the canard cycle is maximal, (10) reduces to

$$\dot{x} = w^{[1/\varepsilon]}, \tag{11a}$$

$$\dot{w} = w\frac{x - q_0}{\gamma_0}. \tag{11b}$$

Noticing that q_0 lies in an ε-neighbourhood of unity, and that canard orbits are exponentially close to the hyperbola $v = \gamma_0(x)$ near the fold, we can approximate the system as

$$\dot{x} \approx -\frac{1}{1+x}, \tag{12a}$$

$$\dot{w} \approx -w(x-1)(x+1). \tag{12b}$$

System (12) is integrable, and provides the following approximation for the solutions of system (11),

$$w \approx K \exp\left(\frac{x^4}{4} + \frac{x^3}{3} - \frac{x^2}{2} - x\right), \tag{13}$$

where K is a constant. In figure 4 we show the phase portrait given by (13) outside the strip $|w| > \delta$. Inside $|w| \ll \delta$, the phase portrait is approximated by vertical fibres with a direction given by the sign of δ. When we discuss the method of pinching in section 4.1, we will show how keen an insight this was, with computed plots that reveal just how sharply the vector field changes between the strip's exterior, $|w| > \delta$, and its interior, $|w| < \delta$.

3. Pinched dynamical systems and sliding

In this section we introduce a piecewise-smooth formulation of multiple time-scale systems, obtained by a method called pinching. We will use this later to complement and extend the analysis in section 2.2. The method of pinching has its origins in [3], where it was used to overcome the lack of uniqueness of orbits in Filippov's description [9] of piecewise-smooth dynamical systems.

Consider a smooth vector field $\mathbf{F} : \mathbb{R}^n \mapsto \mathbb{R}^n$, and the dynamical system

$$\dot{\mathbf{x}} = \mathbf{F}(\mathbf{x}). \tag{14}$$

Let there exist a smooth scalar function $h : \mathcal{U} \mapsto \mathbb{R}$ on an open region $\mathcal{U} \subset \mathbb{R}^n$, such that $\nabla h \neq 0$ everywhere on $\mathcal{U}$. Let h have two level sets labeled

$$\Sigma_\pm = \{\mathbf{x} \in \mathbb{R}^n : h(\mathbf{x}) = \pm\sigma\}, \tag{15}$$

for some $\sigma > 0$, bounding a strip $|h| < \sigma$ which we call the *pinch zone*. (For motivation, consider the pinch zone to be the strip of quasi-vertical flow, $|w| < \delta$, in figure 4). We shall denote by $\dot{h}$ the Lie derivative of h along the flow of (14),

$$\dot{h} = \dot{\mathbf{x}} \cdot \frac{d}{d\mathbf{x}} h(\mathbf{x}) = \mathbf{F} \cdot \nabla h. \tag{16}$$

We wish now to approximate the solutions of $\dot{\mathbf{x}} = \mathbf{F}$ in the pinch zone by some rule that: (i) associates each point on Σ_+ with a point on Σ_-, and (ii) replaces the vector field between them by a suitable approximation.

In the local region $\mathcal{U}$, we can define a surjective map from the pinch zone $|h(\mathbf{x})| < \sigma$, to a *switching manifold* $\Sigma \subset \mathbb{R}^{n-1}$. We do this by choosing fibres $\mathbf{x} = \mathbf{p}_\xi(\lambda)$ that connect the two boundaries Σ_+ and Σ_-, given by

$$\{\mathbf{x} = \mathbf{p}_\xi(\lambda) \ : \ \mathbf{p}_\xi(+1) \in \Sigma_+, \ \mathbf{p}_\xi(-1) \in \Sigma_-, \ -1 < \lambda < 1\}, \tag{17}$$

so that each fibre is associated with (or projected onto) a unique point $\xi \in \Sigma$. Two such fibres are illustrated in figure 5(a). The vector field on Σ is then the set

$$\mathcal{F}_\xi = \{\mathbf{F}(\mathbf{p}_\xi(\lambda)) : -1 < \lambda < 1\}. \tag{18}$$

For simplicity we assume that, for any ξ, the set $\mathcal{F}_\xi$ contains at most one vector that is tangent to a level set of h; we call this a *sliding vector*, and denote it as

$$\mathbf{F}_\mathcal{S}(\xi) = \left\{\mathbf{F}(\mathbf{p}_\xi(\lambda)) : \ \dot{h}(\mathbf{p}_\xi(\lambda)) = 0, \ |\lambda| < 1\right\}. \tag{19}$$

We label the hypersurface $\dot{h} = 0$ as $\mathcal{S}$. For $\mathbf{F}_\mathcal{S}$ to be unique one must have that, for a given ξ, the chord $\mathbf{p}_\xi(\lambda)$ is never tangent to $\mathcal{S}$, hence we choose $\mathbf{p}$ such that the derivative $\partial\dot{h}/\partial\lambda$ is non-vanishing, which we can write as the condition

$$\frac{\partial}{\partial\lambda}\dot{h}(\mathbf{p}_\xi(\lambda)) = \frac{\partial \mathbf{p}_\xi(\lambda)}{\partial\lambda} \cdot \nabla(\mathbf{F}(\mathbf{x}) \cdot \nabla h(\mathbf{x})) \ \neq \ 0. \tag{20}$$

Moreover, if $\mathcal{F}(\xi)$ contains a sliding vector, $\mathbf{F}_\mathcal{S}(\xi)$, then we describe ξ as a *sliding* point, otherwise it is a *crossing* point. Over any open region of sliding points, the sliding vectors form an $n-1$ dimensional vector field, and thus define a dynamical system on Σ given by

$$\dot{\xi} = \mathbf{F}_\mathcal{S}(\xi). \tag{21}$$

Orbits of the pinched dynamical system are defined as the concatenation of:

(i) solutions of equation (14) in the regions $h(\mathbf{x}) > \sigma$ and $h(\mathbf{x}) < -\sigma$, and

(ii) solutions of equation (21) on Σ.

The following theorem follows directly from (19)-(21).

Theorem 3.1. *(a) The boundary between crossing and sliding lies where* $\mathbf{F}$ *is tangent to* Σ_+ *or* Σ_-*. (b) Zeros of* $\mathbf{F}$ *inside the pinch zone correspond to zeros of the sliding vector field* $\mathbf{F}_\mathcal{S}(\xi)$*, which we call* sliding equilibria.

Taking h as a local coordinate, a vector field for the pinched system is obtained by making a piecewise-smooth coordinate transformation $h \mapsto \tilde{h}$, where

$$\tilde{h} = h - \sigma\mathrm{sgn}(h) \ \text{ for } \ |h| > \sigma, \quad \tilde{h} = 0 \ \text{ for } \ |h| \leq \sigma. \tag{22}$$

We say that the sliding region is:

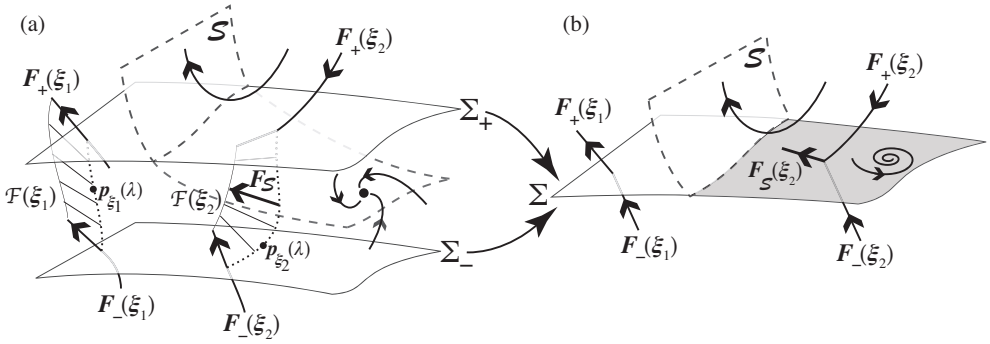

Figure 5. Pinching, and the origin of sliding. (a) A smooth vector field $\mathbf{F}$, and a pinch zone bounded by $\Sigma_\pm$, which are joined by fibres $\mathbf{p}_\xi(\lambda)$. The set-valued vector field $\mathcal{F}(\xi)$ is shown on fibres corresponding to a sliding point ξ_1 and a crossing point ξ_2. Sliding is determined by the positioning of a tangency surface $\mathcal{S}$ (where $\dot{h} = 0$), on which we take the sliding vector $F_{\mathcal{S}}$. Above and below the pinch zone the vector field is approximated by $\mathbf{F}_\pm$. (b) The pinched system around a switching manifold Σ, obtained by pinching together Σ_+ and Σ_-. A tangency of $\mathbf{F}_+$ to Σ bounds sliding (right of $\mathcal{S}$) and crossing (left of $\mathcal{S}$) on Σ.

- stable if $\dot{h}(\mathbf{p}_\xi(+1)) > 0 > \dot{h}(\mathbf{p}(-1;\xi))$ (orbits flow locally towards Σ), and
- unstable if $\dot{h}(\mathbf{p}(-1;\xi)) > 0 > \dot{h}(\mathbf{p}_\xi(+1))$ (orbits flow locally away from Σ).

The intersection of $\mathcal{S}$ with $\Sigma_\pm$ is the locus of points where $\mathbf{F}$ is tangent to Σ_+ or Σ_-. It is this intersection that partitions Σ into regions of sliding or crossing, so the domain of sliding is given by $\mathcal{S} \cap \{\mathbf{x} : |h(\mathbf{x})| < \sigma\}$.

Figure 5 illustrates how the dynamics of a smooth system (a) is approximated, after pinching, by a piecewise-smooth system (b). Orbits that cross both boundaries $\Sigma_\pm$ of the pinch zone in the same direction in (a), are approximated by orbits crossing the switching manifold Σ in (b), while orbits that cross the boundaries in opposite directions in (a) give rise to sliding on the switching manifold in (b). Also illustrated is the content of theorem 3.1, showing that the boundary between crossing and sliding is a tangency between the flow and the pinch zone boundary in (a), corresponding to tangency between the flow and the switching manifold in (b), and showing that an equilibrium inside the pinch zone in (a) is approximated by an equilibrium in the sliding vector field in (b).

3.1. Filippov's sliding vector field

Equation (21) requires knowledge of the exact form of the vector field $\mathbf{F}$ inside the pinch zone, but in many circumstances a further approximation is useful. Recalling that $\mathcal{F}_\xi$ is the set of values of $\mathbf{F}(\mathbf{x})$ along the fibre $\mathbf{p}_\xi(\lambda)$, we can approximate it with a convex set $\tilde{\mathcal{F}}_\xi$, which is an interpolation between the values of $\mathbf{F}$ at the endpoints $\mathbf{p}_\xi(\pm 1)$. Expressing these endpoint values as $\mathbf{F}_\pm(\xi) = \mathbf{F}(\mathbf{p}_\xi(\pm 1))$, we thus have

$$\mathcal{F}_\xi \approx \tilde{\mathcal{F}}_\xi \equiv \left\{ \frac{1+\lambda}{2}\mathbf{F}_+(\xi) + \frac{1-\lambda}{2}\mathbf{F}_-(\xi) : -1 < \lambda < 1 \right\}. \tag{23}$$

This is precisely the convex combination of two vector fields $\mathbf{F}_\pm$ used by Filippov [9] to define sliding on a switching manifold. A sliding vector, which lies on the hypersurface $\mathcal{S}$, is a vector $\tilde{\mathbf{F}} \in \tilde{\mathcal{F}}$ that satisfies $\tilde{\mathbf{F}} \cdot \nabla h = 0$. Assuming that

$\nabla h(\mathbf{p}_\xi(+1)) \approx \nabla h(\mathbf{p}_\xi(-1))$, this occurs at $\lambda = \lambda_\mathcal{S}$, where

$$\lambda_\mathcal{S} = \frac{(\mathbf{F}_- + \mathbf{F}_+) \cdot \nabla h}{(\mathbf{F}_- - \mathbf{F}_+) \cdot \nabla h} \quad ,$$

and therefore the sliding vector field is given by

$$\tilde{\mathbf{F}}_\mathcal{S} = \frac{(\mathbf{F}_- \cdot \nabla h)\mathbf{F}_+ - (\mathbf{F}_+ \cdot \nabla h)\mathbf{F}_-}{(\mathbf{F}_- - \mathbf{F}_+) \cdot \nabla h}. \tag{24}$$

This is formally identical to Fillipov's sliding vector field, and provides us with a piecewise-smooth dynamical system

$$\dot{\mathbf{x}} = \begin{cases} \mathbf{F}_+, & \text{if} \quad h(\mathbf{x}) > \sigma, \\ \tilde{\mathbf{F}}_\mathcal{S}, & \text{if} \quad |h(\mathbf{x})| < \sigma, \\ \mathbf{F}_-, & \text{if} \quad h(\mathbf{x}) < -\sigma. \end{cases} \tag{25}$$

How well (25) approximates the smooth system (14) clearly depends on how the pinch zone $|h| < \sigma$ is chosen. For a slow-fast system such as the van der Pol oscillator (4a) with small ε, we can choose the pinch zone to be a neighbourhood of the critical manifold S_0. Importantly, the interesting quantities we calculate in later sections depend on the geometry of $\mathcal{S}$, which itself depends on the choice of 'pinch function' h, but not on the width of the pinch zone σ.

We will now apply pinching to take a fresh look at some familiar examples of the canard phenomenon, before using it to derive a classification of canards in section 5.

4. Applications of pinching in 2 and 3 dimensions

4.1. Pinching and sliding in the van der Pol oscillator

In this section we use the pinching formalism to analyse canards in the van der Pol oscillator. In figure 6(a) we illustrate a relaxation oscillation simulated from (4) for $\varepsilon = 0.04$. The critical manifold S_0 is given by $h = 0$, where

$$h(x, y) = y - \frac{1}{3}x^3 + x. \tag{26}$$

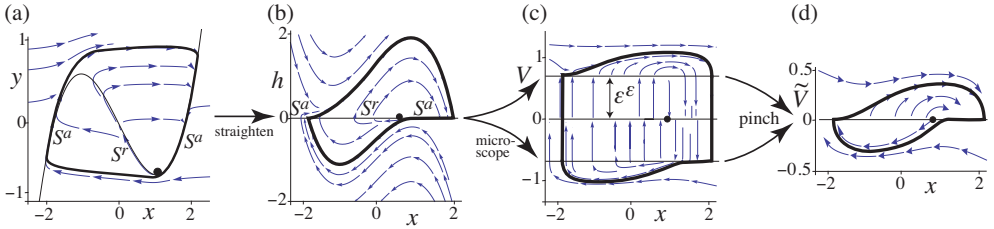

Figure 6. Simulation of (4) for $\varepsilon = 0.04$ and $q = 0.9$, showing the same relaxation oscillation (bold) in four coordinate systems: (a) the Liénard plane (x, y), (b) the plane (x, h), (c) the exponential microscope (x, V), (d) the piecewise-smooth system $(x, \tilde{V})$. The critical manifold, consisting of attracting and repelling branches S^a and S^r, is straightened to give (b), a pinch zone $|V| < \varepsilon^\varepsilon$ emerges around it in (c), which is pinched to a switching manifold $\tilde{V} = 0$ in (d).

If we vary the parameter q from the situation in figure 6(a), there will be no observable change in the segment of periodic orbit lying on the attracting righthand branch of the

critical manifold S^a, prior to its sudden disappearance in a canard explosion (recall figure 2). Thus we attempt to resolve different orbits by proceeding along similar lines to the exponential magnification in section 2.2, but we choose to magnify the Liénard variable y directly instead of using the phase variable $v = \dot{x}$; this has the benefit that x remains the fast variable. First, we simply straighten out the critical manifold S_0 by taking h as a variable, giving the system,

$$\varepsilon \dot{x} = h, \tag{27a}$$

$$\dot{h} = q - x - (x^2 - 1)\frac{h}{\varepsilon}. \tag{27b}$$

The relaxation oscillation from figure 6(a) is shown in the (x, h) plane in figure 6(b). The critical manifold S_0 is now the horizontal axis $h = 0$.

We now attempt to resolve canard orbits by magnifying the neighbourhood of S_0. To do this we introduce a variable

$$V = h^{[\varepsilon]} \equiv \mathrm{sgn}(h)|h|^{\varepsilon}, \tag{28}$$

giving the system

$$\varepsilon \dot{x} = V^{[1/\varepsilon]}, \tag{29a}$$

$$\dot{V} = V\left((1 - x^2) + V^{[-1/\varepsilon]}(q - x)\varepsilon\right), \tag{29b}$$

in which the same relaxation oscillation is plotted in figure 6(c). The critical manifold S_0 remains on the horizontal axis, $V = 0$, and is evidently no longer a local attractor/repeller, but is surrounded by a region, approximately $|V| < \varepsilon^{\varepsilon}$ (corresponding to $|h| < \varepsilon$), where the flow is quasi-vertical. To consider the dynamics relative to this strip, we find the nullcline $\dot{V} = 0$ for $V \neq 0$, given from (29b) by

$$\mathcal{S}_V = \{(x, V) \in \mathbb{R}^2 \ : \ V = \left(\varepsilon(x - q)/(1 - x^2)\right)^{[\varepsilon]}\}. \tag{30}$$

This is shown in figure 7 for different values of q. The curve $\mathcal{S}_V$ becomes singular

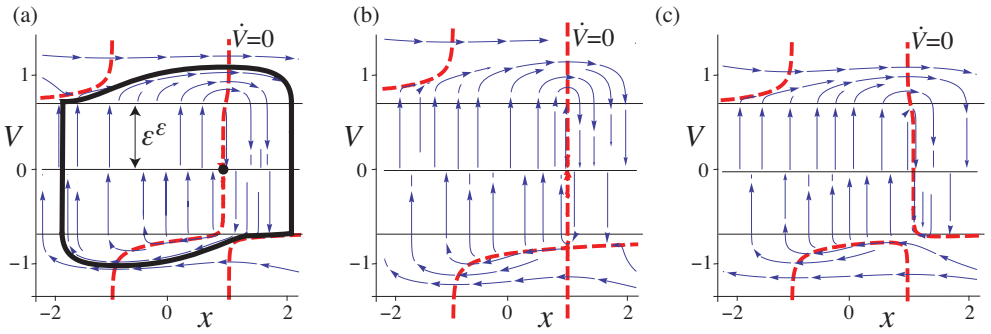

Figure 7. Exponential microscope. Phase portrait of the van der Pol oscillator in the (x, V) magnification, for: (a) $q < 1$, (b) $q = q_V = 1$, (c) $q > 1$. The dashed curve is the nullcline $\dot{V} = 0$.

when $(\partial\dot{V}/\partial x, \partial\dot{V}/\partial V) = (0, 0)$, forming the cross seen in the lower right region of figure 7(b), at a parameter $q = q_V$. From (a) to (c) the nullcline S_V thus undergoes a bifurcation [4] in the form of a saddle transition. Solving $(\partial\dot{V}/\partial x, \partial\dot{V}/\partial V) = 0$ gives the coordinates of the singular point as $(x, V) = (q_V, -(\varepsilon/2)^{\varepsilon})$, and substituting this into (29b) gives $q_V = 1$, which therefore coincides with the Hopf bifurcation in

the original system. The relaxation oscillation in figure 7(a) disappears in a canard explosion between (a) and (b).

We now derive a piecewise-smooth approximation from (29) by following section 3, to arrive at figure 6(d). It is natural to choose a pinch zone $|V| < \varepsilon^\varepsilon$ (equivalently $|h| < \varepsilon$), inside which the vector field is near vertical. We will pinch along the V-direction (setting $\mathbf{p}$ in section 3 as $\mathbf{p}_x(\lambda) = (x, \lambda\varepsilon^\varepsilon)$). The vertical fibration of the pinch zone by the flow implies that this is a good approximation to the dynamics. This is equivalent to introducing a new coordinate as in (22), given by $\tilde{V} = V - \varepsilon^\varepsilon \mathrm{sgn}(V)$. From section 3, sliding occurs at x values for which the nullcline $\mathcal{S}_V$ ($\dot{V} = 0$) lies in

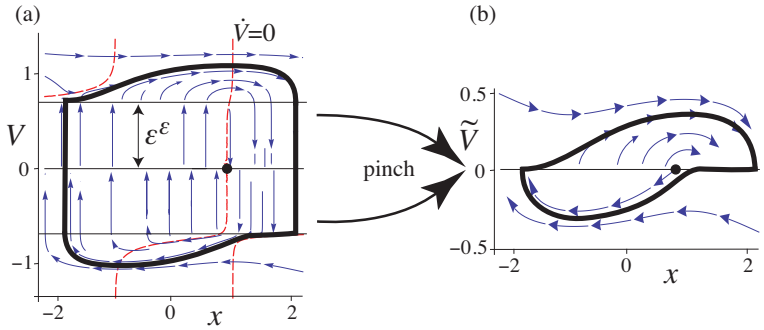

Figure 8. Relaxation oscillation in: (a) the (x, V) magnification, (b) the piecewise-smooth system obtained by pinching the region $|V| < \varepsilon^\varepsilon$ in (a). Plotted for the same parameter values as figure 6(a). S_0 is the $V = 0$ axis, the dashed curve is the nullcline $\dot{V} = 0$ corresponding to $\dot{h} = 0$.

the pinch zone. From (30), the sliding region is therefore given by

$$|V| = \left|\frac{x-q}{1-x^2}\right|^\varepsilon \varepsilon^\varepsilon < \varepsilon^\varepsilon \quad \Rightarrow \quad |x-q| < |1-x^2|, \tag{31}$$

on the switching manifold $\tilde{V} = 0$. The sliding vector field has an equilibrium at $x = q$. The boundaries of sliding, where the vector field is tangent to the switching manifold, are therefore where $|x - q| = |1 - x^2|$. The tangencies to the upper and lower side of the manifold are labeled T_1 and T_2 respectively in figure 9. The critical manifold S_0 has become the switching manifold, with stable sliding corresponding to the attracting manifold S^a, and unstable sliding corresponding to the repelling manifold S^r, as shown.

It is not necessary to calculate the sliding vector field explicitly (though it is easily found from (24)), as we can infer it qualitatively from two facts: firstly that the stability of the sliding equilibrium (stable for $|q| < 1$ and unstable for $|q| > 1$), and secondly that, from (24), the sliding vector field is equal to the upper vector field at T_1 and to the lower vector field at T_2.

Inspection of the piecewise-smooth vector field in figure 9(a) makes it clear that a relaxation oscillation occurs because an orbit, sliding towards T_2 from the right, will detach from the manifold at T_2, pass through the manifold near $x = -1$, and then be re-injected into the sliding region from above. The bifurcation of the curve $\mathcal{S}_V$ at $q = 1$ causes the tangency points to collide in figure 9(b). Then the crossing region (dotted) between T_1 and T_2 shrinks to nothing, and a canard orbit exists that passes from the stable to unstable sliding regions (from S^a to S^r). Every point on the unstable sliding region S^r belongs to a family of orbits that travel along S^r for some time,

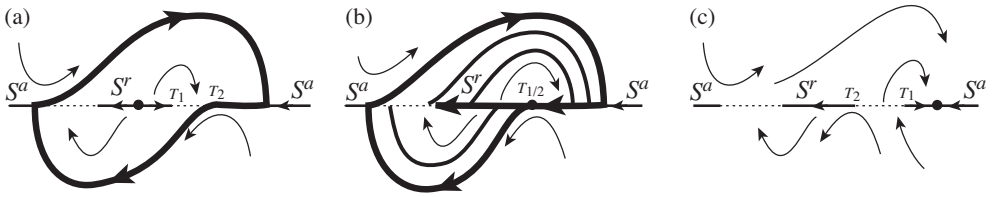

Figure 9. Sketch of the bifurcation responsible for the canard explosion: (a) relaxation oscillation at $q < 1$, (b) the simple canards at $q = 1$, (c) stable sliding equilibrium at $q > 1$. The upper and lower vector fields are tangent to the switching manifold at T_1 and T_2 respectively. These bound the sliding regions (horizontal lines) and crossing regions (dotted horizontal lines). The black spot is the sliding equilibrium, unstable in (a) and stable in (c). S^a and S^r label the stable and unstable sliding regions, approximating stable and unstable slow manifolds of system (29).

before departing into either the upper or lower half planes and being reinjected into S^a; every one of these is a periodic orbit and constitutes an instantaneous 'snapshot' of the entire canard explosion. When the tangency points separate in figure 9(c), orbits in the righthand sliding region are attracted to the sliding equilibrium and no periodic orbits are possible. Thus the bifurcation that takes place in figure 9 describes the sudden disappearance of the relaxation oscillation, via the instantaneous existence of a family of canard cycles at $q = 1$. In section 5 we will classify this as the *simple canard* case of a *catastrophic sliding bifurcation*.

Let us now show that the same method can split the instant $q = 1$ into two families of canards: those in figure 9(b) that detach from the upper side of the switching manifold (without head) and those that detach from the lower side (with head).

Whereas in figures 6 (a) and (b) the cycle (bold) appears to lie on an attracting branch S^a of the critical manifold as it approaches the fold, we see from figure 7(a), in which S^a lies on the axis $V = 0$, that the cycle lies instead on the curve $\dot{V} = 0$. Let us therefore approximate the canard by the curve S_V when $q = 1$. Solving $\dot{h} = 0$ (equivalent to $\dot{V} = 0$) for $q = 1$, from (27b), confirms the result that led to (8), that near the knee of S_0 at $(x, y) = (1, -2/3)$, the canard is given by

$$h \approx \varepsilon\gamma_0(x) \equiv -\varepsilon\frac{1}{1+x}. \tag{32}$$

To magnify the phase portrait around this curve in the h-direction we use a different exponential scaling, introducing the variable

$$W = (h - \varepsilon\gamma_0(x))^{[\varepsilon]}, \tag{33}$$

and obtaining the system

$$\dot{x} = \frac{1}{\varepsilon}W^{[\frac{1}{\varepsilon}]} + \gamma_0(x), \tag{34a}$$

$$\dot{W} = |W|^{1-\frac{1}{\varepsilon}}\left(\left[W^{[\frac{1}{\varepsilon}]} + \varepsilon\gamma_0(x)\right]\left[(1-x^2) - \varepsilon\gamma_0^2(x)\right] + (q-x)\varepsilon\right). \tag{34b}$$

The relaxation oscillation in the (x, W) plane is illustrated in figure 10(a). The focus, which in the (x, V) plane resided inside the pinch zone, has now been lifted outside. Compare this to figure 4(a), which is restricted to $-1 < x < 2$ and a vertical range that excludes the focus; the variable W differs from the analysis of Benoît et al leading to (8) by a scaling $W = \varepsilon^{\varepsilon}w$. Notice that the vector field, while vertical in the region given approximately by $|W| < \varepsilon^{2\varepsilon}$, changes direction as it passes through the nullcline

$\dot{W} = 0$. As q changes from (a) to (c) in figure 10, the nullcline segment inside the pinch zone sweeps to the right, changing the vertical vector field direction from downward to upward.

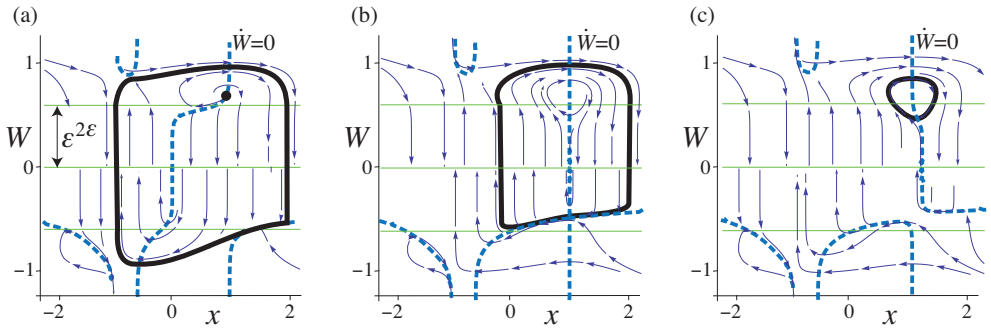

Figure 10. Second exponential microscope. Phase portrait of the van der Pol oscillator in the (x, W) magnification, for: (a) $q < q_W$, (b) $q = q_W$, (c) $1 > q > q > W$. The dashed curve is the nullcline $\dot{V} = 0$. Compare the region $x > 0$ to figure 4.

The nullcline $\dot{W} = 0$ is given from (34b) by

$$\mathcal{S}_W = \left\{ (x, W) \in \mathbb{R}^2 \ : \ W = \left(\frac{x - q}{1 - x^2 - \varepsilon\gamma_0^2(x)} - \gamma_0(x) \right)^{[\varepsilon]} \varepsilon^{\varepsilon} \right\}. \quad (35)$$

Similar to the bifurcation of the nullcline S_V at $q = 1$, the curve S_W becomes singular at some parameter $q = q_W$, forming a cross as shown in figure 10(b). This takes place when $(\partial\dot{W}/\partial x, \partial\dot{W}/\partial W) = 0$, the solution of which gives the coordinates of the singularity as

$$(x, W) = \left(q_W, \ -\left(\frac{3\varepsilon^2}{2(1 + q_W)\left(q_W(1 + q_W)^3 - \varepsilon\right)} \right)^{[\varepsilon]} \right), \quad (36)$$

and substituting these into $\dot{W} = 0$ gives the bifurcation parameter $q = q_W$ as the solution of

$$\varepsilon = (1 - q_W)(1 + q_W)^3. \quad (37)$$

Similarly to the (x, V) system, we now define a pinch zone given by $|W| < \varepsilon^{2\varepsilon}$ in which the vector field is almost vertical. We pinch vertically, in this case by defining a new variable $\tilde{W} = W - \varepsilon^{2\varepsilon}\mathrm{sgn}W$, and in the $(x, \tilde{W})$ plane we obtain a piecewise-smooth system as shown in figure 11. We omit the details for calculating the sliding dynamics on the switching manifold $\tilde{W} = 0$, as the steps are similar to those for the $(x, \tilde{V})$ system, and because the necessary information can be inferred directly from (34)-(35).

The vector field is tangent to the switching manifold at the x-values where the curve (35) enters the pinch region. We label them T_1 and T_2 for the tangency to the upper and lower side of the switching manifold respectively. As illustrated in figure 12, for $q < q_W$, T_1 lies to the left of T_2, with stable sliding to the right of T_2. This allows a periodic orbit to exist as simulated in figure 11(b) and sketched in figure 12(a). As the nullcline $\dot{W} = 0$ bifurcates, at $q = q_W$ given by (37), the two tangencies collide. A canard orbit then passes from the stable to unstable sliding regions, and since every

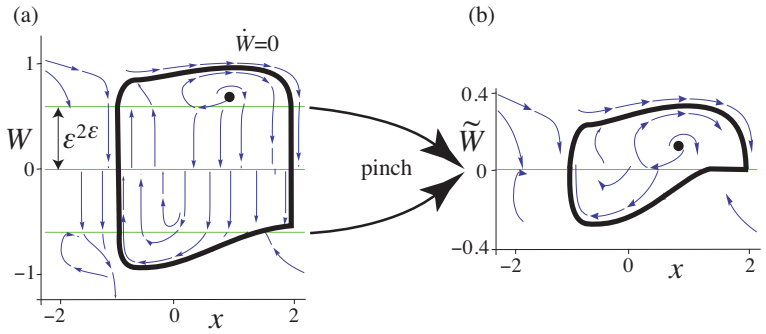

Figure 11. Relaxation oscillation in: (a) the (x, W) magnification, (b) the piecewise-smooth system obtained by pinching the region $|W| < \varepsilon^{2\varepsilon}$ in (a). Plotted for the same parameter values as figure 6(a). The dotted curve is the nullcline $\dot{W} = 0$.

point in the unstable sliding region belongs not only to an orbit in the sliding region, but also to orbits departing into both the upper and lower half planes, every one of these is also a periodic orbit and constitutes an instantaneous 'snapshot' of a canard explosion. This explosion is not the one observed in the (x, V) plane, figure 9, because it terminates not in a stable focus, but in the small periodic orbit shown in figure 12(c). This, instead, is a cascade between the canard with head in figure 12(a) and the canard without head in figure 12(c). In section 5 we will classify this as the *visible canard* case of a *catastrophic sliding bifurcation.*

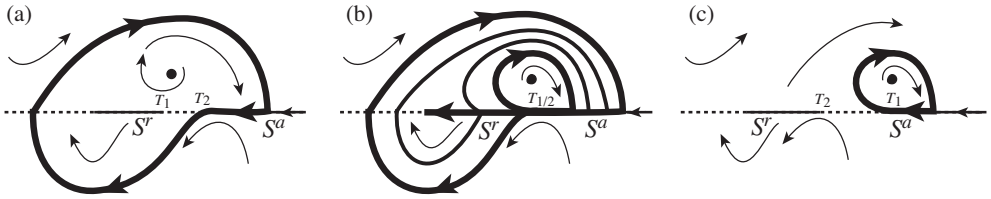

Figure 12. Sketch of the bifurcation responsible for the transition between canards with and without head: (a) a large cycle corresponds to the canard with head at $q = q_W - 10^{-4}$, (b) the visible canard at $q = q_W$, (c) a small cycle corresponds to the canard without head at $q = q_W + 10^{-4}$. The upper and lower vector fields are tangent to the switching manifold at fold points T_1 and T_2 respectively; these exchange exchange ordering in the bifurcation. S^a and S^r label the stable and unstable sliding regions, approximating stable and unstable slow manifolds of system (34).

Previously we assigned the value $q = q_0$ to the maximal canard, which marks the transition between canards with and without head. The bifurcation of the $\dot{W} = 0$ nullcline at $q = q_W$ signifies a change in curvature of the flow, from pushing orbits upwards to pushing them downwards relative to the maximal canard at $W = 0$. Therefore q_W gives us a geometrical approximation for the value $q = q_0$ at which the maximal canard occurs, $q_0 = q_W$, and hence from (37) we obtain a quartic expression for q_0:

$$\varepsilon = (1 - q_0)(1 + q_0)^3. \tag{38}$$

Thus the bifurcation in figure 12 controls the disappearance of a large cycle (figure 12(a)) to be replaced by a small cycle (figure 12(c)), via an instantaneous canard cascade at $q = q_W$.

For $q \approx q_0$ we can use an observation of [1] that led to (10b), namely that we can rewrite (34a) using the following result which is proved in the Appendix:

Lemma 5.1 [1] *The ordinary differential equation (34b) can be rewritten as*

$$\frac{1}{W}\dot{W} = \frac{x - q_0}{\gamma_0} + \frac{q - q_0}{W^{[1/\varepsilon]}}\varepsilon. \tag{39}$$

Using this lemma, we can approximate for $q - q_0$ sufficiently small,

$$\dot{x} \approx \gamma_0(x), \tag{40a}$$

$$\dot{W} \approx W\frac{x - q_0}{\gamma_0(x)}. \tag{40b}$$

Replacing the lefthand side of (40b) with $\dot{W} = \dot{x}\frac{dW}{dx} = \gamma_0(x)W\frac{d\log W}{dx}$, we can solve to find

$$W(x) \approx W(0)\exp\left(-q_0 x - \frac{2q_0 - 1}{2}x^2 + \frac{1}{3}x^3 + \frac{1}{4}x^4\right) \tag{41}$$

as first found in [1] and recounted in (13), except that here q_0 is included with the value (38)) instead of approximation by unity. This gives an approximate expression for the trajectories of canards in the region $|W| > \varepsilon^{2\varepsilon}$.

This can be improved using the pinched piecewise-smooth system, because the vector fields in the half planes $\tilde{W} > 0$ and $\tilde{W} < 0$ are independent. In particular we can make independent approximations in either half plane. We linearize about the equilibrium in the upper half plane, and expand for small $\tilde{W}$ in the lower half plane (where there are no equilibria), and also expand about $x = 1$, to obtain

$$\dot{x} \approx -\frac{1}{2} + H(W)W^{[1/\varepsilon]}/\varepsilon, \tag{42a}$$

$$\dot{W} \approx 2W\left((q_0 - x) + H(W)(q - q_0)\left(1 - \frac{2}{\varepsilon}W^{[1/\varepsilon]}\right)\right), \tag{42b}$$

where $H(W)$ equals 1 if $W > 0$ and 0 if $W < 0$. This adds a correction to (40) outside $|W| > \varepsilon^{2\varepsilon}$ that captures the focus in the upper half plane, and captures the exchange of tangency points responsible for the canard. Using the pinching method, we have thus derived a piecewise-smooth system, (42), that captures the geometry behind the canard explosion in figure 12 and extends the nonstandard analysis summarized in section 2.2.

Let us briefly review what information about the singularly perturbed system has been captured by pinching. The exchange of tangency points T_1 and T_2 in figures 9 and 12 enacts a discontinuity-induced bifurcation – bifurcations of the periodic orbits caused by interaction with the discontinuity at $V = 0$ or $W = 0$. These cases are catastrophic forms of *sliding bifurcations* [16], whose classification we will present in section 5. These sliding bifurcations in the (pinched) piecewise-smooth system correspond to bifurcations in the topology of the nullclines $\dot{V} = 0$ and $\dot{W} = 0$ in the smooth system, coinciding with the Hopf bifurcation and maximal canard respectively.

4.2. Pinching and sliding in the Fitzugh-Nagumo equations

We now extend the analysis of the previous section, where an oscillator underwent a supercritical Hopf bifurcation, to a case involving a subcritical Hopf bifurcation. As a specific example we take an abstract form of the FitzHugh-Nagumo equations [10] used to model electrical excitations in nerve membranes. Written in terms of a membrane voltage potential v and recovery variable w, setting $f(v) = \beta v^3 + (1+\alpha)v^2 - \alpha v$ and $g = g(v, w)$ affine, these take the form

$$\varepsilon \dot{v} = \beta v^3 + (1+\alpha)v^2 - \alpha v - w + I, \tag{43a}$$

$$\dot{w} \ = bv - cw, \tag{43b}$$

where α, β, I, are parameters and b, c, are constants. This is equivalent to (3) up to a simple coordinate translation,

$$x = v - \frac{1+\alpha}{3\beta}, \qquad y = \frac{I-w}{3\beta} - f\left(\frac{1+\alpha}{3\beta}\right), \tag{44}$$

giving (3) with $f(x) = \frac{1}{3}x^3 - rx$ and $g(x, y) = q - px - y$, to obtain

$$\varepsilon \dot{x} = y - \frac{1}{3}x^3 + rx, \tag{45a}$$

$$\dot{y} \ = q - px - y. \tag{45b}$$

The critical manifold S_0 of this system is the curve $h = 0$, where

$$h(x, y) = y - \frac{1}{3}x^3 + rx. \tag{46}$$

The form of S_0 depends on r, and we fix $r > 0$ so that S_0 has two turning points (where $f'(x) = 0$), at $(x, y) = \pm\sqrt{r}(1, -\frac{2}{3})$. Throughout this section we will keep r and p fixed and vary q as a bifurcation parameter.

The dynamics depends upon the number of equilibria of (45). These occur at $(x_{\rm eq}, y_{\rm eq})$ where $x_{\rm eq}$ is a solution of $\frac{1}{3}x_{\rm eq}^3 + (p-r)x_{\rm eq} - q = 0$. The number of solutions depends on the discriminant $\Delta = (3q/2)^2 + (p-r)^3$. If $\Delta < 0$ there are 3 equilibria, and a stable cycle that can be destroyed by homoclinic connection to a saddle. In this section we restrict attention to the simpler case with one focus, $\Delta > 0$, so we fix

$$\Delta = (3q/2)^2 + (p-r)^3 > 0. \tag{47}$$

The flow is illustrated in figure 13. A relaxation oscillation exists in (a). It is subsequently destroyed, but by a different process to that in section 4.1. There is a focus equilibrium which in (a) lies on the unstable branch S^r of S_0. The focus changes stability in a subcritical Hopf bifurcation, creating an unstable cycle as shown (dotted) in figure 13(b). The unstable cycle undergoes a canard explosion, and (b) captures an instant in the sequence of canards. In this system, the unstable canard is without head and grows in amplitude, while the stable canard is with head and shrinks in amplitude. In (c), the two cycles coincide at a parameter $q = q_0$ to be determined, and annihilate in a saddle-node bifurcation of cycles. At $q = q_0$, the two cycles coincide and we observe numerically that these are close to a maximal canard (dotted). Afterwards, in (d), the cycles are destroyed, leaving a stable focus on S^a.

We will not go into as much detail as the previous section, and instead seek only to derive the mechanism by which the cycles are destroyed in figure 13(c), following the

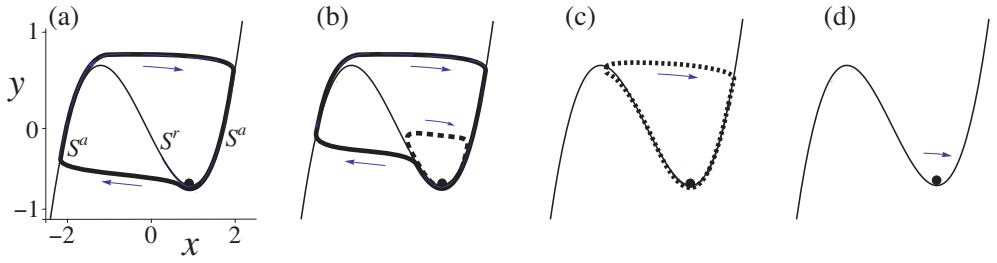

Figure 13. Simulation of (45) for $\varepsilon = 0.04$. Plots are with $p = r = 1$ and q values: (a) $q_0 - 0.02$, (b) $q_0 - 6.045 \times 10^{-5}$, (c) q_0, (d) $q_0 + 0.02$. The cubic curve is S_0 given by $\dot{x} = h = 0$, with attracting branches S^a and repelling branch S^r. Stable (bold) and unstable (dotted) periodic orbits are shown around a focus (spot). The maximal canard parameter q_0 is to be determined.

same steps as in section 4.1. We first straighten out S_0 by transforming to coordinates (x, h), giving the system

$$\varepsilon \dot{x} = h, \tag{48a}$$

$$\dot{h} \ = \eta_p(x) + \frac{1}{\varepsilon}\eta'_\varepsilon(x)h, \tag{48b}$$

in terms of the function

$$\eta_\lambda(x) \equiv h(x, q - \lambda x) = -\frac{1}{3}x^3 + (r - \lambda)x + q, \tag{49}$$

and its derivative $\eta'_\lambda(x) = r - \lambda - x^2$. The nullcline $\dot{h} = 0$ is the curve $h = \varepsilon\gamma(x)$, where

$$\gamma(x) \equiv -\eta_p(x)/\eta'_\varepsilon(x). \tag{50}$$

This nullcline bifurcates when $\partial\dot{h}/\partial x = \partial\dot{h}/\partial h = 0$. Solving these we find that the bifurcation takes place at coordinates

$$(x, h) = (x_h, h_h) \equiv \left(\pm\sqrt{r - \varepsilon},\ \frac{\varepsilon(\varepsilon - p)}{2x_h}\right), \tag{51}$$

and substituting these coordinates back into $\dot{h} = 0$ we find the bifurcation parameter value to be

$$q = q_h \equiv \frac{1}{3}x_h^3 + (p - r)x_h. \tag{52}$$

This coincides with the value of q at which an subcritical Hopf bifurcation takes place.

We can magnify the strip $|h| < \varepsilon$ by rescaling to a coordinate $V = h^{[\varepsilon]}$ as in (28), obtaining

$$\varepsilon \dot{x} = V^{[1/\varepsilon]}, \tag{53a}$$

$$\dot{V} \ = |V| \left(\eta'_\varepsilon(x) + \varepsilon V^{[-1/\varepsilon]}\eta_p(x)\right), \tag{53b}$$

then derive a pinched system to approximate it. The piecewise-smooth system obtained at this level is identical to figure 9, that is, the unstable cycle belongs to the infinite number of coexisting periodic orbits at $q = q_h$, none of which can be distinguished as either stable or unstable. As before, to distinguish between different canards we must magnify around the maximal canard.

The maximal canard, similarly to section 4.1, is found to lie on the curve given by the nullcline $\dot{h} = 0$ when $q = q_h$. We therefore let $\gamma_0(x)$ be the function $\gamma(x)$ from (50) with $q = q_h$, and approximate the maximal canard by $h \approx \varepsilon\gamma_0(x)$, where

$$\gamma_0(x) \equiv -\frac{\eta_p(x) + q_h - q}{\eta'_\varepsilon(x)} = -\frac{1}{3}\left(x + \frac{3p - 2r - \varepsilon}{x \pm \sqrt{r - \varepsilon}}\right). \tag{54}$$

The nullcline $\dot{V} = 0$ bifurcates at the same parameter $q = q_h$ as the nullcline $\dot{h} = 0$.

To magnify around this maximal canard curve, we rescale to a coordinate $W = (h - \varepsilon\gamma_0(x))^{[\varepsilon]}$, obtaining

$$\dot{x} \;= \frac{1}{\varepsilon}W^{[1/\varepsilon]} + \gamma_0(x), \tag{55a}$$

$$\dot{W} = |W|^{[1-\frac{1}{\varepsilon}]}\left([\eta'_\varepsilon(x) - \varepsilon\gamma'_0(x)][W^{[\frac{1}{\varepsilon}]} + \varepsilon\gamma_0(x)] + \varepsilon\eta_d(x)\right), \tag{55b}$$

where $\gamma'_0(x) = [2x\gamma_0(x) + (p - r + x^2)]/(r - \varepsilon - x^2)$.

The nullcline $\dot{W} = 0$ bifurcates when $\partial\dot{W}/\partial x = \partial\dot{W}/\partial W = 0$, which we solve to find the bifurcation coordinates $(x, W) = (x_0, W_0)$. For the same reasoning as in section 4.1, this bifurcation takes place approximately when the maximal canard is formed. We find that x_0 is a solution of

$$\eta'_\varepsilon(x_0) - \varepsilon f'_0(x_0) = 0, \tag{56}$$

which can be solved numerically, or expanded as a Taylor series to find

$$x_0 \approx x_h + \frac{3\varepsilon(2r - p - \varepsilon)}{4(r - \varepsilon)(6r - 7\varepsilon)}x_h \;+\; \mathcal{O}\left[(x_0 - x_h)^2\right] \tag{57}$$

and, exactly,

$$W_0 = \left(-\varepsilon\gamma_0(x_0) - \frac{\eta'_p(x_0)}{\frac{1}{\varepsilon}\eta''_\varepsilon(x_0) - \gamma''_0(x_0)}\right)^{[\varepsilon]}. \tag{58}$$

Substituting these into $\dot{W} = 0$ we find the bifurcation parameter $q = q_0$ at which the maximal canard exists to be given by

$$q_0 = \frac{1}{3}x_0^3 + (r - p)x_0. \tag{59}$$

Simulations in this case are similar to figure 11(a), except that they reveal an unstable cycle around a stable focus as shown in figure 14(a) for $q < q_0$. At q_0 in (b), the tangencies T_1 and T_2 of the upper and lower vector fields to the switching manifold collide, allowing a canard orbit to pass from the stable to unstable sliding regions, giving rise to a family of canard cycles. As for the supercritical van der Pol system, we have canards with head that depart from the underside of the unstable sliding region, and canards without head that depart from the upper side, but now these correspond to the cascades of stable and unstable canards, one of which is the maximal canard. Afterwards, for $q > q_0$ in (c), the piecewise-smooth system contains no mechanism by which a periodic orbit can exist, as all orbits are attracted towards the stable focus.

Similarly to the supercritical van der Pol system, the bifurcation in the pinched system will be classified in section 5 as a visible canard case of catastrophic sliding bifurcation. We could go on to consider similar systems, such as replacing (45b) with $\dot{y} = q - px + y$, in which a supercritical Hopf bifurcation is followed by a canard explosion that can be interrupted by a homoclinic connection to a saddle. In such a case, it might be appropriate to perform an exponential magnification around the stable manifold of the saddle to determine when it becomes part of a canard. Instead of considering further such extensions, let us now turn our attention to canards in three dimensions.

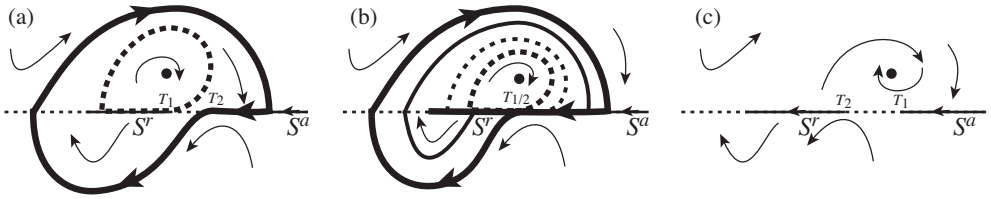

Figure 14. Sketch of the bifurcation responsible for the stable and unstable canard explosions in the subcritical van der Pol system: (a) a stable cycle (bold) with head and unstable cycle (dotted) without head at $q = q_0 - 10^{-4}$, (b) a visible canard exists at the maximal canard parameter $q = q_0$, (c) no periodic orbits exist for $q = q_0 + 10^{-4}$. The upper and lower vector fields are tangent to the switching manifold at fold points T_1 and T_2 respectively; these exchange exchange ordering in the bifurcation.

4.3. Two fast variables in three dimensions: the Hindmarsh-Rose burster

We now give an example of pinching in a three dimensional system. Unsurprisingly the analysis is more involved in three dimensions, and it is beyond the scope of this paper to investigate such a system in detail. We give only a brief introduction to the analysis that can be carried out, taking the Hindmarsh-Rose equations [13] as an example.

A slow-fast system in $\mathbb{R}^3$ with two fast variables has a fast subsystem that is two-dimensional. This allows for the possiblity of periodic motion in the fast dynamics, which can induce bursting oscillations in the full system [15]. The Hindmarsh-Rose equations are a classic example of a simple bursting system, and can be written as

$$\varepsilon \dot{x} = z - f(x) + I - y, \tag{60a}$$

$$\dot{y} \;\; = s(x - x_1) - y. \tag{60b}$$

$$\varepsilon \dot{z} = g(x) - z, \tag{60c}$$

where $f(x) = ax^3 - bx^2$ and $g(x) = c - dx^2$. Here x represents a voltage variable and y a slowly varying current, giving a slow-fast system of the form (3), to which we add a fast variable z and applied current I, see [12] for more details. We take typical values $a = 1$, $b = 3$, $c = 1$, $d = 5$, and $s = -1.618$, that are known to be physically relevant.

This model exhibits spiking behaviour. One can observe by numerical simulation that periodic bursting attractors are formed by an alternation between rapid phases, containing a number of spikes, and slow resting phases. Parameter-dependent families of periodic orbits are known to exist and display a spike-adding phenomenon. In the following we consider branches of periodic attractors obtained upon variation of I, but a similar spike-adding phenomenon exists when I is fixed and ε is varied. At low I-values, the unique stable equilibrium of the system undergoes a Hopf bifurcation where a branch of stable periodic attractors is born at the point labelled y_{sp} in figure 15. The Hopf point is located very close to one fold of the v-nullcline and the subsequent periodic orbit follows the unstable (middle) branch of this cubic nullcline. Hence these periodic orbits are of canard type and the phenomenon is reminiscent of a canard explosion. For increasing I-values, the associated periodic orbit stays close to the unstable branch for a longer time, until eventually it remains close long enough to reach the upper fold point. This is consistent with the notion of a maximal canard. Shortly after this, as I increases, the associated periodic orbit starts to develop a fast oscillation – a spike. Hence the spike's appearance is suggested to be canard-induced,

and it is found that the process repeats itself again and again, as I increases, each time adding an extra fast spike, as shown in figure 15.

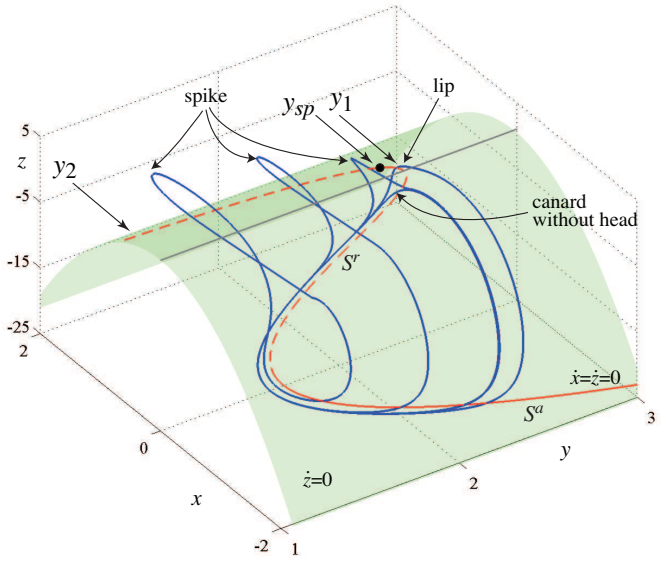

Figure 15. Periodic attractors of the Hindmarsh-Rose model (60), for different values of the applied current I. The quadratic surface $\dot{z} = 0$ is shown, and contains the cubic curve $S_0 = S^a \cup S^r$, the family of equilibria of the associated fast subsystem, which undergoes a Hopf bifurcation at the point marked $y = y_{sp}$. A canard cycle without head is shown, and follows S_0. The cycle grows into a maximal canard, developing a 'lip' as it passes over the fold of the quadratic surface. When the cycle grows beyond the Hopf point it leaves the surface and grows a spike that winds around S_0 via the fast subsystem.

We now demonstrate how the analysis of previous sections can be used, by applying the exponential microscope followed by pinching, to derive the birth of the first spike. For a general analysis of the spike-adding phenomenon in terms of slow manifolds of saddle type and the relative position of their (un)stable manifolds, see [11].

Non-spiking cycles remain close to the parabolic surface $\dot{z} = 0$, so we begin by considering only the dynamics therein. (A stronger case for this is when the fast subsystem itself has two time-scales, so that (60) read $\varepsilon_1 x = ...$, $y = ...$, $\varepsilon_2 z = ...$, with $\varepsilon_1 \ll \varepsilon_2 \ll 1$, and we can restrict to the fast subsystem by setting $\varepsilon_2 = 0$. This subsystem itself has slow-fast time-scales with ratio $\varepsilon = \varepsilon_1/\varepsilon_2 \ll 1$. In effect, the small parameter ε pushes the Hopf bifurcation point in the fast subsystem in the direction of decreasing z. Recalling that the Hopf point initiates spiking, this causes the periodic attractor of the full system to lose its burst, following instead a small oscillation via the fast subsystem; such a periodic attractor resembles a canard with head where the orbit leaves the vicinity of the repelling branch of the cubic nullcline and relaxes onto the attracting branch by oscillating around it.)

Let us then begin by fixing to the surface $y = c - dx^2$, upon which the dynamics

is given by

$$\varepsilon\dot{x} = c + I - y - ax^3 + (b-d)^2, \tag{61a}$$

$$\dot{y} \ = s(x - x_1) - y. \tag{61b}$$

As for a planar system, we then straighten out the cubic curve where $\dot{x} = 0$ by replacing y with the coordinate $h = \varepsilon\dot{x}$, obtaining

$$\varepsilon\dot{x} = h, \tag{62a}$$

$$\dot{h} \ = \eta_d(x) + h\left(\frac{1}{\varepsilon}\eta_d(x) - 1\right), \tag{62b}$$

where

$$\eta_\lambda(x) = c + I - ax^3 + (b-\lambda)x^2. \tag{63}$$

The nullcline $\dot{h} = 0$ bifurcates when $0 = \dot{h} = \partial\dot{h}/\partial x = \partial\dot{h}/\partial h$, with solution $0 = \eta_d(x) = \eta_d'(x) - \varepsilon = \varepsilon s + 2h(b-d) - 2h\varepsilon/x$, giving

$$x_h = \frac{1}{3a}\left(1 \pm b - d \pm \sqrt{(b-d)^2 - 3a\varepsilon}\right), \tag{64a}$$

$$h_h = \ \mp \varepsilon s/2\sqrt{(b-d)^2 - 3a\varepsilon}, \tag{64b}$$

$$I_h \ = ax_h^3 - (b-d)x_h^2 - I. \tag{64c}$$

At the parameter $I = I_h$, a Hopf bifurcation takes place (as is confirmed by a simple stability analysis). The maximal canard closely follows the curve given by the nullcline $\dot{h} = 0$ when $I = I_h$, that is $h = \varepsilon\gamma_0(x)$, where

$$\gamma_0(x) = \frac{\eta_d(x)}{\varepsilon - \eta_d'(x)}. \tag{65}$$

In the previous two sections we then magnified the strip $|h| < \varepsilon$. Let us omit this (as we found it does not distinguish different canards from each other), and instead magnify around the maximal canard by introducing the variable $W = (h - \varepsilon\gamma_0(x))^{[\varepsilon]}$, giving the system

$$\dot{x} \ = \frac{1}{\varepsilon}W^{[1/\varepsilon]} + \gamma_0(x), \tag{66a}$$

$$\dot{W} = |W|^{1-\frac{1}{\varepsilon}}\left([\eta_d'(x) - \varepsilon - \varepsilon\gamma_0'(x)][W^{[\frac{1}{\varepsilon}]} + \varepsilon\gamma_0(x)] + \varepsilon\eta_d(x)\right). \tag{66b}$$

The nullcline bifurcates when $0 = \dot{W} = \partial\dot{W}/\partial x = \partial\dot{W}/\partial W$, the solution of which gives

$$I_0 = ax_0^3 - (b-d)x_0^2 - I, \tag{67}$$

where x_0 is a solution of

$$\eta_d'(x_0) - \varepsilon\gamma_0'(x_0) = \varepsilon, \tag{68}$$

and, for completeness, we have also

$$W_0 = \left(\frac{\varepsilon\eta_d'(x_0)}{\gamma_0''(x_0) - \eta_d''(x_0)} - \varepsilon\gamma_0(x_0)\right)^{[\varepsilon]}. \tag{69}$$

Beyond this value of I_0, the canard develops a head that remains, for a short range of parameters, on the parabolic surface $\dot{z} = 0$. We can estimate this parameter range as follows. Let $\delta I = I_0 - I_h$, then the canards without head exist over the parameter range $I_0 - \delta I < I < I_0$. The canard with head can exist over a similar range the other

side of I_0, that is, $I_0 < I < I_0 + \delta I$, during which the head grows over the region $y_2 < y < y_1$, where $y_1 = I + c$ and $y_2 = c + I + \left(\frac{2}{a}\right)^2 \left(\frac{b-d}{3}\right)^3$. The head does not reach full size, however, being interrupted by the Hopf point of the fast subsystem and developing a spike. Let us say that this takes place at $y = y_{sp}$, shown in figure 15. If each spike grows linearly with I up to y_2, then spike growth takes place over a parameter range $I_{sp} < I < I_{sp} + \frac{y_2 - y_{sp}}{y_2 - y_1}\delta I$, and is preceded by a 'lip' — the canard briefly growing a head — over a range $I_0 < I < I_{sp}$. If we assume that the growth of the head with I is approximately linear, then

$$I_{sp} \approx I_0 + \frac{y_{sp} - y_1}{y_2 - y_1}\delta I. \tag{70}$$

It remains to find the value $y = y_{sp}$ at which the fast subsystem undergoes a Hopf bifurcation by solving $\dot{x} = \dot{y} = 0$ and $\partial\dot{x}/\partial x + \partial\dot{y}/\partial y = 0$, giving $y_{sp} = I + c - ax_{sp}^3 + (b-d)x_{sp}^2$, where $x_{sp} = \left(b - \sqrt{b^2 - 3a}\right)/3a$.

Finally, it is possible to capture the creation of the first spike via the canard explosion, by using an exponential microscope and looking at bifurcations of level sets associated with the flow. A complete description of the spike-adding phenomenon in such bursters, the necessary exponential rescalings, and the bifurcations of level sets, is beyond the primarily expository scope of this paper; these will be addressed in future work. We turn now to a more general result, a local classification of the different forms of canards that are possible in systems of arbitrary dimension.

5. Classification of canards in piecewise-smooth systems

Recently, a class of discontinuity-induced bifurcations affecting periodic orbits have been classified in piecewise-smooth systems. In [16], it was stated that these "catastrophic sliding bifurcations" included a classification of three generically occuring canards. We will show here how these can be derived from singularly perturbed systems by the method of pinching.

In a neighbourhood of one of the folds $\{f'(x) = 0\}$ of the critical manifold S_0 in (4), we can neglect terms cubic in $(x-1)$ and, after a simple change of variables, write

$$\varepsilon\dot{x} = y - \frac{1}{2}x^2, \tag{71a}$$

$$\dot{y} \ = q - x. \tag{71b}$$

This expresses a slow-fast system with a critical manifold S_0 given by $y = \frac{1}{2}x^2$, in the neighbourhood of a fold point at the origin. We can use pinching to derive a piecewise-smooth approximation to this system. Let $h = y - \frac{1}{2}x^2$, so that the critical manifold is $h = 0$, and choose a neighbourhood, $|h| < \sigma$ for some $\sigma > 0$, to form a pinch zone. The nullcline $\dot{h} = 0$, labeled $\mathcal{S}$ in section 3, is given by $\mathcal{S} = \left\{(x, \frac{1}{2}x^2 + \varepsilon\left(\frac{q}{x} - 1\right)) \ : \ x \in \mathbb{R}\right\}$.

We can pinch in the y-direction along fibres (17) given by $\mathbf{p}_x(\lambda) = (x, \frac{1}{2}x^2 + \sigma\lambda)$. This is equivalent to defining a new coordinate $\tilde{y} = y - \sigma\mathrm{sgn}(h)$ which, by substitution into (71), satisfies the piecewise-smooth system

$$\dot{x} = \frac{\sigma}{\varepsilon}\mathrm{sgn}(\tilde{y} - \frac{1}{2}x^2) + \mathsf{O}\left(\tilde{y}, x^2\right), \tag{72a}$$

$$\dot{\tilde{y}} = q - x. \tag{72b}$$

From (19), we can derive a sliding vector field $\mathbf{F}_{\mathcal{S}} = \frac{q-x}{x}(1, x)$ on the switching manifold $\tilde{y} = \frac{1}{2}x^2$. This appears to be divergent at $x = 0$, but from section 3, it

only applies on the sliding region, for which $\left|\frac{q}{x}-1\right| < \frac{\sigma}{\varepsilon}$, hence the point $x = 0$ does not lie in this region so the divergence is never encountered. The boundaries are the tangencies of the upper vector field to the switching manifold at T_1, where $x = q/(1+\sigma/\varepsilon)$, and of the lower vector field at T_2, where $x = q/(1-\sigma/\varepsilon)$, where the vector field curves respectively towards and away from the manifold. There is a sliding equilibrium (a point where $\mathbf{F}_{\mathcal{S}} = 0$) at $x = q$.

If we plot the phase portrait in the (x, h) coordinates for varying q we arrive at figure 16(a). Consider if the orbit marked $\star$ (for $q < 0$) is the local segment of a periodic orbit that detaches from the manifold at T_1. Let q increase: the tangencies collide when $q = 0$, at which point the orbit can pass from the stable to unstable sliding regions; we call this a *simple canard*. For $q > 0$ the orbit terminates at the sliding equilibrium, hence the periodic orbit has vanished, but has done so instantly (or catastrophically).

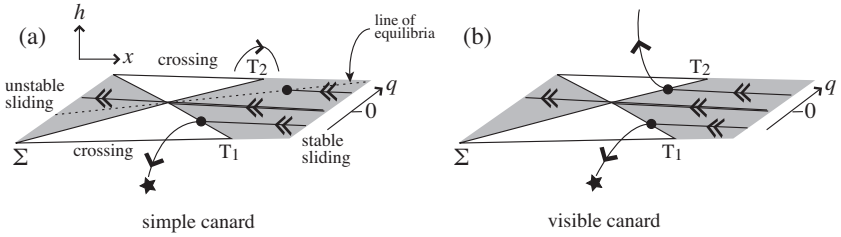

Figure 16. Types of canard in two dimensions, as the parameter q varies. A small change of inset causes a jump in the outset. We classify these as: (a) simple canard, (b) visible canard.

Notice that the tangencies T_1 and T_2 in figure 16(a) are such that the vector fields curve locally downward, confirmed by verifying that $\ddot{h} < 0$ in the flows of (71). More generally in a piecewise-smooth system, the sign of $\ddot{h}$ can be positive at both tangencies, or different at each, so the vector field can curve towards or away from the manifold. When all possible scenarios are considered, it is easily verified (provided $\ddot{h} \neq 0$, see [9] or [16]) that there are two other cases in which an orbit passes from stable sliding to unstable. One of these is uninteresting, because the flows either side of the manifold both curve towards it, keeping the flow within a neighbourhood of the manifold. The interesting case is shown in figure 16(b). Here, an orbit with a tangency to the manifold is visible on both sides of the canard parameter, hence we call this a *visible canard*.

The double tangency point through which the canard trajectory passes is not generic in two dimensions, and is only seen under variation of a parameter (such as q). In three dimensions, however, tangencies occur along curves, and generically these can cross to form double tangencies. We now show how these are derived from a singular perturbation problem.

Consider the three dimensional system:

$$\varepsilon\dot{x} = y - \frac{1}{2}x^2, \tag{73a}$$

$$\dot{y} = bz + cx, \tag{73b}$$

$$\dot{z} = a, \tag{73c}$$

which is a local normal form for a three dimensional system with a slow variable added to (71) [23]. As above, we can let $h = y - \frac{1}{2}x^2$, define a pinch zone $|h| < \sigma$, and

pinch along the y-direction by defining a coordinate $\tilde{y} = y - \sigma\mathrm{sgn}(h)$, which satisfies a piecewise-smooth system

$$\dot{x} = \frac{\sigma}{\varepsilon}\mathrm{sgn}(\tilde{y} - \frac{1}{2}x^2) + \mathsf{O}\left(\tilde{y}, x^2\right), \tag{74a}$$

$$\dot{\tilde{y}} = bz + cx, \tag{74b}$$

$$\dot{z} = a. \tag{74c}$$

The sliding vector field $\mathbf{F}_{\mathcal{S}}$ is given on $\tilde{y} = \frac{1}{2}x^2$ by

$$\dot{x} = (bz + cx)/x \tag{75a}$$

$$\dot{z} = a. \tag{75b}$$

This can be recognised from [23] as similar to the slow subsystem of (73) when $\varepsilon = 0$. Notice, however, that this piecewise-smooth approximation has been obtained for *nonzero* ε. The sliding region is given by $|(bz + cx)/x| < \sigma/\varepsilon$, which excludes the line $x = 0$ where (75a) is singular. The boundaries of the sliding region are where the vector fields in (74) are tangent to the switching manifold $\tilde{y} = 0$. They lie along $z = (\pm\frac{\sigma}{\varepsilon} - c)x/b$, labeled T_1 and T_2 in figure 17. These lines cross at the origin, and the sliding vector field is not well defined there.

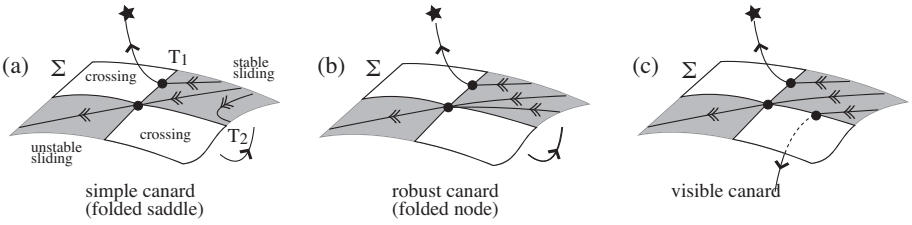

Figure 17. The 3 canards in three dimensions. A small change of inset causes a jump in the outset. We classify these as: (a) simple canard, (b) robust canard, (c) visible canard. Their corresponding classification in singularly perturbed systems [23] is indicated in brackets, noting that (c) seems not to have appeared previously in the singular perturbation literature. The vector field is tangent to the upper side of the switching manifold along T_1, and to the lower side along T_2. An extra arrow in (a)-(b) shows that the vector field curves towards the manifold around T_2.

We can infer the phase portrait of the sliding vector field by considering the desingularised system $(x\dot{x}, x\dot{z})$, which has at the origin: a saddle if $ab > 0$, a focus if $ab < ab + \frac{1}{4}c^2 < 0$, and a node if $ab < 0 < ab + \frac{1}{4}c^2$; the focus/node is attracting if $c < 0$ and repelling otherwise. We need then to observe that the equilibrium of the desingularized system $(x\dot{x}, x\dot{z})$ is not a true sliding equilibrium (that is $\mathbf{F}_{\mathcal{S}}$ is not zero, and not even uniquely defined, at the origin). Note that the x-factor reverses flow direction in the unstable sliding region in the desingularization, and that orbits in $\mathbf{F}_{\mathcal{S}}$ can reach the origin in finite time. These facts are usually indicated by adding the term "folded" to denote the origin as a "folded-node", "folded-saddle", etc. (degenerate cases arise at the marginal parameter values $ab + \frac{1}{4}c^2 = 0$ and $abc = 0$, but these are nongeneric); see [23, 27]. Thus we arrive at two generalizations of the simple canard (figure 16(a)) in three dimensions, shown in figure 17(a)-(b). Both cases require that the Jacobian matrix $\begin{pmatrix} c & b \\ a & 0 \end{pmatrix}$ of the desingularised sliding vector field $(x\dot{x}, x\dot{z})$ has

two eigenvectors in the sliding region, which is satisfied if $c^2 + 4ab > 0$ and

$$\sigma/\varepsilon > \left(c + \left\{2ab/\left(c \pm \sqrt{c^2 + 4ab}\right)\right\}\right)^2, \tag{76}$$

which is found by requiring that the righthand sides of (74), for the different signs in (74a), both point towards or both away from the switching manifold $h = 0$. The simple canard, figure 17(a), arises from the saddle-like sliding vector field ($ab > 0$). A robust case, figure 17(b), arises from the attractive node-like sliding vector field ($c < 0$, $ab < 0$, $c^2 + 4ab > 0$), and is so-named because a whole one-parameter family of canard orbits exist.

These were classified from piecewise-smooth systems theory in [16], in which a third type of canard was introduced. Notice that, in figure 17(a)-(b), one vector field curves towards the switching manifold (along T_2) while the other curves away from it (along T_1). This is the situation so long as $(ab - \sigma^2/\varepsilon^2)^2 > c^2\sigma^2/\varepsilon^2$, and hence is always true if σ/ε is sufficiently small. More generally, however, the vector fields could both curve towards the manifold (if $c\sigma/\varepsilon \pm \left(ab - \sigma^2/\varepsilon^2\right) < 0$) or both away from it ($c\sigma/\varepsilon \pm \left(ab - \sigma^2/\varepsilon^2\right) > 0$). Canards are possible in both cases, but only in the latter case can they depart the switching manifold in such a way that they can form one-parameter families of periodic orbits – these are the only ones of interest for canard explosions. The canard arises when the sliding vector field is saddle-like ($ab > 0$) with only one eigenvector in the sliding region ((76) is satisfied for only one of the signs $\pm$). This we call the visible case (figure 17(c)), and generalises the visible canard from figure 16(b).

Figure 17 illustrates the phase portraits around the "sliding canards" that are generic in piecewise-smooth systems. Consider the orbits marked $\star$ to be local segments of periodic orbits, and allow their inset to change as a parameter varies (similar to figure 16, but this time the local vector field does not change with the parameter). Then observe that when a periodic orbit deforms such that it passes through a double tangency point, it first forms a canard, and then, because its local curvature changes discontinuously, the periodic orbit will be destroyed. These belong to a larger class of four discontinuity-induced transitions called "catastrophic sliding bifurcations" [16], the fourth of which we omit since it does not involve a canard.

Figure 17 thus provides a classification of piecewise-smooth canards in three dimensions. Furthermore, in [16] it is shown that these form a classification in $\mathbb{R}^n$ for $n \geq 3$. It is interesting to remark that the local sliding vector fields which give rise to this classification appear already in Filippov's seminal text on piecewise-smooth systems [9]. Figure 16 provides their extension to planar systems, and in sections 4.1-4.3 we showed that piecewise-smooth systems, derived from slow-fast systems by the pinching method of section 3, typically exhibit the canard types classified above.

A note of caution must be given on the unfortunate terminology that has arisen for this same singular point, in the different fields of singularly perturbed and discontinuous dynamical systems. The singularity lying at the origin of (73), namely a non-hyperbolic point on a slow manifold, is called a *fold* (and in a addition a folded-node, folded-saddle, etc. depending on the slow dynamics), see e.g. [23]. The corresponding singularity lying at the origin of (74), namely a quadratic tangency of a piecewise smooth flow to both sides of a switching manifold, is known as a *two-fold* singularity, (this is because a quadratic tangency to only one side of the switching manifold is known as a *fold*), see e.g. [17].

6. Concluding remarks

In this paper, we revisited the canard phenomenon in singularly perturbed dynamical systems, showing a close geometrical link between nonstandard analysis and piecewise-smooth methods. We first reviewed the exponential microscope approach of Benoît et al. [1], which allows the dynamics associated with a canard explosion to be resolved locally. We then showed that similar results can be obtained in the framework of piecewise-smooth dynamical systems using the concept of pinching. The exponential microscope renders the vector field almost vertical close to the critical manifold, providing an obvious choice of pinch zone, and we analyzed the parameter values where canards and maximal canards occur. We also applied these techniques to a three-dimensional burster, the Hindmarsh-Rose system, to analyse the transition from basic canard cycles to canards with one spike. The same mechanism can be found in other three-dimensional bursters (such as the Morris-Lecar equations [25]) and has been recently studied from the standpoint of invariant manifolds, in particular, slow manifolds of saddle-type and their (un)stable manifolds [11]. We have shown that pinching can be used to study the transition from canard cycles to spiking periodic attractors.

The method of pinching introduced in section 3, and applied to canards in sections 4.1-5, can be used more generally to approximate singularly perturbed systems by piecewise-smooth vector fields. In particular, we have used it to describe the dynamics around non-hyperbolic (fold) points of critical manifolds, where the Fenichel theory of normally hyperbolic invariant manifolds breaks down. This is an alternative to blow-up methods, which focus on regaining hyperbolicity by introducing an extended system.

Pinching can be seen as the converse to regularization, where a piecewise-smooth system is smoothed out at the switching manifold. It has been shown only recently, in [24], that the regularisation of a piecewise-smooth system is topologically equivalent to a singularly perturbed system, and that sliding orbits are homeomorphic to dynamics on a slow manifold. This result assumes normal hyperbolicity of the slow manifold, and therefore does not yet apply in the neighbourhood of non-hyperbolic points, such as those giving rise to the canards we are interested in (the resolution of this will again require blow-up methods). Ongoing and future work include the study of how well pinching can capture the full range of canard phenomena in $\mathbb{R}^3$, such as mixed-mode dynamics [22, 20], small amplitude oscillations near the fold [5], and spike-adding mechanisms [11].

Complementing this use of flow curvature to characterise canards, is the classification of canards derived from piecewise-smooth (or pinched) systems in figure 17. A canard occurs where regions of stable sliding and unstable sliding meet at a point. The dynamics in a stable sliding region is non-unique in reverse time, while the dynamics in an unstable sliding region is non-unique in forward time (recall figure 5(b)). When the two come together, orbits can be channeled from stable to unstable dynamical regions, creating the enormous sensitivity to initial conditions responsible for the suddenness of a canard explosion.

Appendix: Proof of Lemma 5.1

Given the system in (34),

$$\varepsilon\dot{x} = W^{[1/\varepsilon]} + \varepsilon\gamma_0(x)$$

$$\dot{W} = W^{[1-\frac{1}{\varepsilon}]}\left(\left[W^{[1/\varepsilon]} + \varepsilon\gamma_0(x)\right]\left[(1-x^2) - \varepsilon\gamma_0^2(x)\right] + (q-x)\varepsilon\right),$$

we differentiate along an orbit,

$$\frac{dW}{dx} = \varepsilon(h-\varepsilon\gamma_0)^{[\varepsilon]-1}\left(h'(x) - \varepsilon\gamma_0'(x)\right) \tag{77}$$

$$= \varepsilon W^{1-\frac{1}{[\varepsilon]}}\left[h'(x) - \varepsilon\gamma_0'(x)\right] \tag{78}$$

where

$$h'(x) = \frac{\dot{h}}{\dot{x}} = \frac{\varepsilon(q-x) + h(1-x^2)}{h} = \frac{\varepsilon}{h}(q-x) + 1 - x^2. \tag{79}$$

To find $\gamma_0'(x)$, note that $\varepsilon\gamma_0$ is a solution of (34) when $q = q_0$, so

$$\varepsilon\gamma_0'(x) = h'(x)|_{q=q_0} = \frac{1}{\gamma_0}(q_0 - x) + 1 - x^2. \tag{80}$$

Substituting the difference between (79) and (80) into (77), we have

$$\frac{dW}{dx} = \varepsilon W^{1-\frac{1}{[\varepsilon]}}\left[\frac{\varepsilon}{h}(q-x) - \frac{1}{\gamma_0}(q_0 - x)\right] \tag{81}$$

and straightforward manipulation of the term in square brackets gives

$$\begin{aligned}
[\cdot] &= \left(\frac{1}{\gamma_0} - \frac{\varepsilon}{h}\right)x + \left(\frac{\varepsilon}{h}q - \frac{q_0}{\gamma_0}\right) \\
&= \left(\frac{1}{\gamma_0} - \frac{\varepsilon}{h}\right)(x - q_0) + \left(\frac{\varepsilon}{h}q - \frac{q_0}{\gamma_0}\right) + q_0\left(\frac{1}{\gamma_0} - \frac{\varepsilon}{h}\right) \\
&= \frac{h - \varepsilon\gamma_0}{\gamma_0 h}(x - q_0) + \varepsilon\frac{q - q_0}{h} \\
&= \frac{W^{1/[\varepsilon]}}{\varepsilon\dot{x}}\left(\frac{x - q_0}{\gamma_0} + \varepsilon\frac{q - q_0}{W^{1/[\varepsilon]}}\right).
\end{aligned} \tag{82}$$

Finally, substituting this into (81) we have the result of Lemma 5.1,

$$\dot{W} = \dot{x}\frac{dW}{dx} = W\left(\frac{x - q_0}{\gamma_0} + \varepsilon\frac{q - q_0}{W^{1/[\varepsilon]}}\right). \qquad \square \tag{83}$$

References

[1] E. Benoît, J.-L. Callot, F. Diener and M. Diener. *Chasse au Canard.* Collect. Math. **32**: 37–119, 1981.

[2] M. Brøns and K. Bar-Eli *Canard explosion and excitation in a model of the Belousov-Zhabotinskii reaction.* J. Phys. Chem. **95**(22): 8706–8713, 1991.

[3] M. E. Broucke and C. C. Pugh and S. N. Simić *Structural stability of piecewise smooth systems.* Comput. Appl. Math. **20**: 51-90, 2001.

[4] M. Demazure, *Bifurcations and catastrophes: geometry of solutions to nonlinear problems*, Springer, 2000.

[5] M. Desroches, J. Guckenheimer, B. Krauskopf, C. Kuehn, H. M. Osinga and M. Wechselberger *Mixed-mode oscillations in systems with multiple time-scales.* to appear in SIAM Review (in press), 2010.

[6] M. Desroches and M. R. Jeffrey *Canards and curvature: the "smallness of ε" in slow-fast dynamics*, Proc. R. Soc. A, in review, 2011.

[7] N. Fenichel, *Persistence and smoothness of invariant manifolds for flows.* Indiana Univ. Math. J. **21**:193–226, 1971-1972.

[8] N. Fenichel, *Geometric singular perturbation theory for ordinary differential equations.* J. Differential Equations **31**(1):53–98, 1979.

[9] A. F. Filippov, *Differential Equations with Discontinuous Righthand Sides.* Kluwer, 1988.

[10] R. FitzHugh, *Impulses and physiological states in theoretical models of nerve membrane.* Bioophys. J. **1**:445–466, 1961.
[11] J. Guckenheimer and C. Kuehn, *Computing slow manifolds of saddle type.* SIAM J. Appl. Dyn. Syst. **8**(3):854–879, 2009.
[12] J. L. Hindmarsh and P. Cornelius *The development of the Hindmarsh-Rose model for bursting.* In Bursting: The Genesis of Rythm in the Nervous System (S. Coombes and P. C. Bressloff eds), World Scientific, 2005, pp.3–18.
[13] J. L. Hindmarsh and R. M. Rose *A model of neuronal bursting using three coupled first-order differential equations.* Proc. R. Soc. Lond. **B 221**:87-102, 1984.
[14] M. W. Hirsch, C. C. Pugh and M. Shub *Invariant manifolds.* Lecture Notes in Mathematics Vol.**583**, Springer-Verlag, Berlin, 1977.
[15] E. Izhikevich, *Neural excitability, spiking, and bursting.* Int.J.Bifur.Chaos **10**:1171–1266, 2000.
[16] M. R. Jeffrey and S. J. Hogan *The geometry of generic sliding bifurcations* SIAM Review (accepted), 2011
[17] M. R. Jeffrey and A. Colombo *The two-fold singularity of discontinuous vector fields* SIAM J. Appl. Dyn. Syst., 8: 624–640, 2009
[18] C. K. R. T. Jones *Geometric singular perturbation theory* In Dynamical systems (Montecatini Terme, 1994), Lecture Notes in Math. **1609**: 44–118, Springer (Berlin), 1995
[19] T. J. Kaper *An introduction to geometric methods and dynamical systems theory for singular perturbation problems* In Analyzing multiscale phenomena using singular perturbation methods (Baltimore, MD, 1998), Proc. Sympos. Appl. Math. **56**: 85–131, Amer. Math. Soc. (Providence, RI), 1999
[20] M. Krupa, N. Popović and N. Kopell *Mixed-Mode Oscillations in Three Time-Scale Systems: A Prototypical Example.* SIAM J. Appl. Dyn. Syst. **7**(2): 361–402, 2008.
[21] A. Liénard, *Etude des oscillations auto entretenues.* Revue Générale de l'Electricité **23**: 901–946, 1928.
[22] N. Popović, *Mixed-mode dynamics and the canard phenomenon: Towards a classification.* J. Phys.: Conf. Ser. **138**: 012020, 2008.
[23] P. Szmolyan and M. Wechselberger *Canards in R^3.* J. Differ. Equ. **177**: 419-453, 2001.
[24] M. A. Teixeira and J. Llibre and P. R. da Silva *Regularization of Discontinuous Vector Fields on $\mathbb{R}^3$ via singular perturbation.* J. Dyn. Diff. Equat.**19**: 309-331, 2007.
[25] D. Terman *Chaotic spikes arising from a model of bursting in excitable membranes.* SIAM J. Appl. Math. **51**(5): 1418–1450, 1991.
[26] B. Van der Pol *On "relaxation oscillations".* Phil. Mag. Ser. 7 **2**(11): 978–992, 1926.
[27] M. Wechselberger *Existence and bifurcation of canards in $\mathbb{R}^3$ in the case of a folded node.* SIAM J. Appl. Dyn. Syst. **4**(1): 101–139, 2005.
[28] M. Wechselberger *Canards.* Scholarpedia **2**: 1356, 2007.